Hydrodynamics and Scale-up of Coal Liquefaction Reactor

小野崎, 正樹
九州大学工学応化機能材料物性工学

https://doi.org/10.11501/3172442

出版情報：九州大学, 2000, 博士（工学）, 課程博士
バージョン：
権利関係：

5. A Simulation of the Accumulation of Solid Particles in Coal Liquefaction Reactors.

1. The Nature of the Solid Particles

5.1 Introduction

In each run, the pressure drop between the top of the reactor and the inlet line connected to the bottom of the reactor gradually increased with passing operation time as shown in Figure 3-1. The accumulation of solid particles reduced the effective volume of the reactor. Slurry samples withdrawn from the reactor contained particles, which were from a few μm to about 500 μm in diameter. Ueda et al. [1] and Aramaki and the author et al.[2] investigated the structure of relatively large particles recovered from the Kashima pilot plant. Those particles were composed of a core which contained SiO_2 as the major component and FeS and Al_2O_3 as minor components, in addition to a peripheral region which contained $CaCO_3$, FeS, and $MgCO_3$. It was also reported by Aramaki and the author et al.[3] that these particles were found in the high-pressure / high-temperature separator at the downstream of the reactor and in the downstream pipes.

Sedimentation of solids has been also reported in other direct coal liquefaction reactors. Wakeley et al.[4] found that particles recovered from a coal dissolver at the Wilsonville SRC pilot plant were largely calcium carbonate particles which were 50-150 μm in diameter. Each particle was composed of a distinct layer, surrounding the core. Okuma et al.[5] analyzed sediments in a liquefaction reactor using Victorian brown coal and found that the solids were multi-layered carbonates of Ca, Mg and Na. Mochizuki et al.[6] analyzed deposits from reactors of PSU, which was designed and operated based on the NEDOL Process (capacity, 1 ton of coal per day; reactor dimensions, 0.175 m in diameter and 1.75 m in height). The cores of these particles contained Si and Al, and the concentric shells outside of the cores were largely composed of Ca. The accumulation rate of solids from Wyoming coal with a high Ca content increased with increasing reaction temperature, but no effect of reaction temperature was observed for Illinois No.6 coal with a low Ca content.

Thus, sedimentation of solid deposits in liquefaction reactors is greatly dependent on reaction conditions and coal

types, but the specific role of each factor in the sedimentation has not been investigated. The objective of the present study[7] is to characterize the solid deposits in the reactors at the Kashima pilot plant. The hydrodynamics of particle sedimentation in the reactors based on the population balances, which include entrainment, growth, and axial dispersion of solid particles, is discussed in Chapter 6.

5.2 The operation of the Kashima Pilot Plant and Analysis of Solid Particles

Figure 5-1 shows a trend of operation for 60 days including three major cases, in which the continuous operation was performed. The operating conditions are shown in Table 2-2. After allowing 9 days for start-up, the conditions of case 2 were maintained for 18 days, and the conditions of case 3 were maintained for 11 days. Finally, the coal concentration was increased to about 50 wt%, and the conditions for case 4 were maintained for 15 days.

Figure 5-1 also shows the sampling sequence. A total of 6 samples were withdrawn from the reactors during the operation through nozzles (B) (middle) and (C) (bottom) of the first reactor, and a total of 6 samples through nozzle (B) of the second and third reactors during the operation. Each sample was withdrawn into a high pressure container which was 0.0164 m^3 in size, and the slurry was depressurized into a low-pressure container using a needle valve. After cooling, the liquid and solid were separated, and the solid particles were washed with hexane. The morphology of the solid particles was observed using a scanning electron microscope (SEM), and size distributions were determined with a laser diffractiometer using a suspension of the samples in ethanol under ultrasonic irradiation. The crystallinity of the particles was determined by polarization microscopy, and the elements were determined by x-ray spectrometry and energy dispersive X-ray spectrometry (EDX).

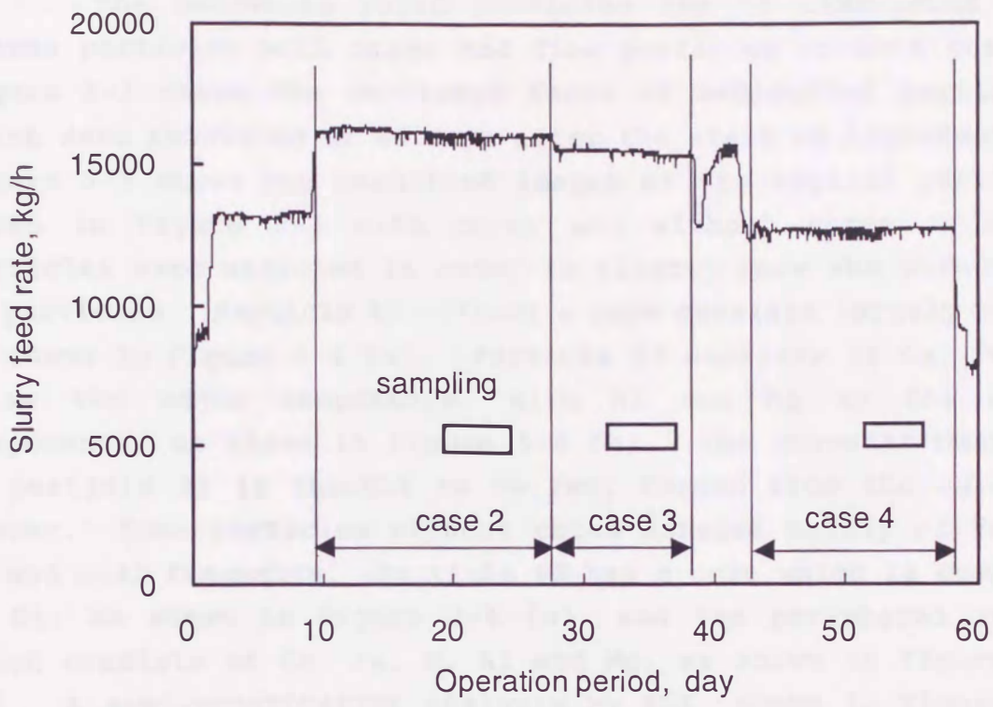

Figure 5-1. Operating conditions and timings of the sampling.

5.3 Properties of the Solid Particles

The recovered solid particles can be classified into coarse particles with cores and fine particles without cores[2]. Figure 5-2 shows the sectioned faces of sedimented particles, which were recovered at 40 days after the start of liquefaction. Figure 5-3 shows the magnified images of the typical particles shown in Figure 5-2 with cores and without cores. Larger particles were selected in order to clearly show the structures of particles. Particle #1 without a core consists largely of Si, as shown in Figure 5-4 (a). Particle #2 consists of Ca, Fe and S as the major components, with Al and Mg as the minor components, as shown in Figure 5-4 (b). The granular material in particle #2 is thought to be FeS, formed from the catalyst powder. Some particles without cores consist mainly of Fe, S, Al and coal fragments. Particle #3 has a core which is composed of Si, as shown in Figure 5-4 (c), and the peripheral region which consists of Ca, Fe, S, Al and Mg, as shown in Figure 5-4 (d). A semi-quantitative analysis by EDX shown in Figure 5-5 is consistent with the X-ray spectrometry data. An ultimate analysis shows that the sedimented solid particles, which were larger than 500 μm in diameter, were composed of approximately 90 wt% of CaO and 0.4 wt% of SiO_2. The particles which were smaller than 500 μm in diameter were compositionally 8-17 wt% of CaO and 30-60 wt% of SiO_2. The solid particles were not always spherical, and the cores assumed a variety of shapes, including cylinders and long spheroids. The size of the particles with cores was largely in the range of 10-200 μm, and that of the cores was largely in the range of 1-80 μm (the peak of frequencies of size = approximately 25 μm). The size of particles without cores was also in the range of 1-80 μm. The average density of the solid particles was determined to be 2700 kg m^{-3}.

As shown in Figure 5-6, the calcium content of the particles which were recovered from the first reactor increased, while the iron content decreased, with increasing operation periods. However, the calcium content in the samples recovered

from the second and third reactors remained constant with respect to the operation period, as shown in Figure 5-7. The iron content in the cores were higher than that in the peripheral zones. These results suggest that the particle growth was caused mainly by the deposition of calcium compounds on the cores. The particles which were recovered at PSU[6] showed a structure similar to that of the particles recovered at the Kashima pilot plant. Most particles recovered at the Victorian brown-coal liquefaction plant[5] had no cores and consisted of multi-layers of carbonates. Those recovered at the Wilsonville SRC plant[4] had the cores composed of semi-coke and pyrrhotite and the peripherals composed of calcium carbonate and pyrrhotite. The above differences in particle structures can be attributed, in part, to differences in the composition and reactivity of the coals used in each plant. The operation conditions for liquefaction also affect the properties of the accumulated particles, as described in Chapter 6.

Figure 5-2. Global SEM image of particles.

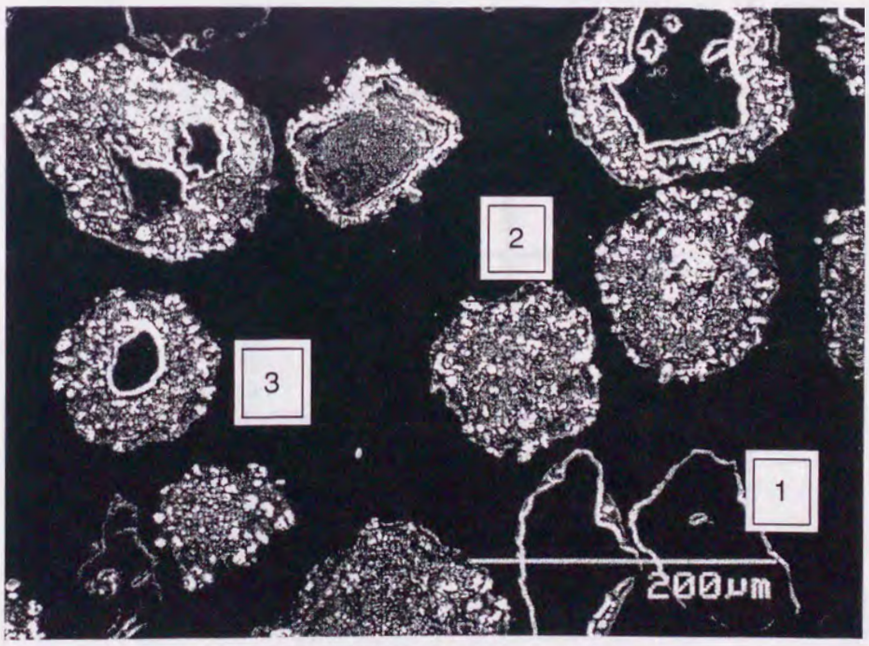

Figure 5-3. Magnified SEM image of particles.

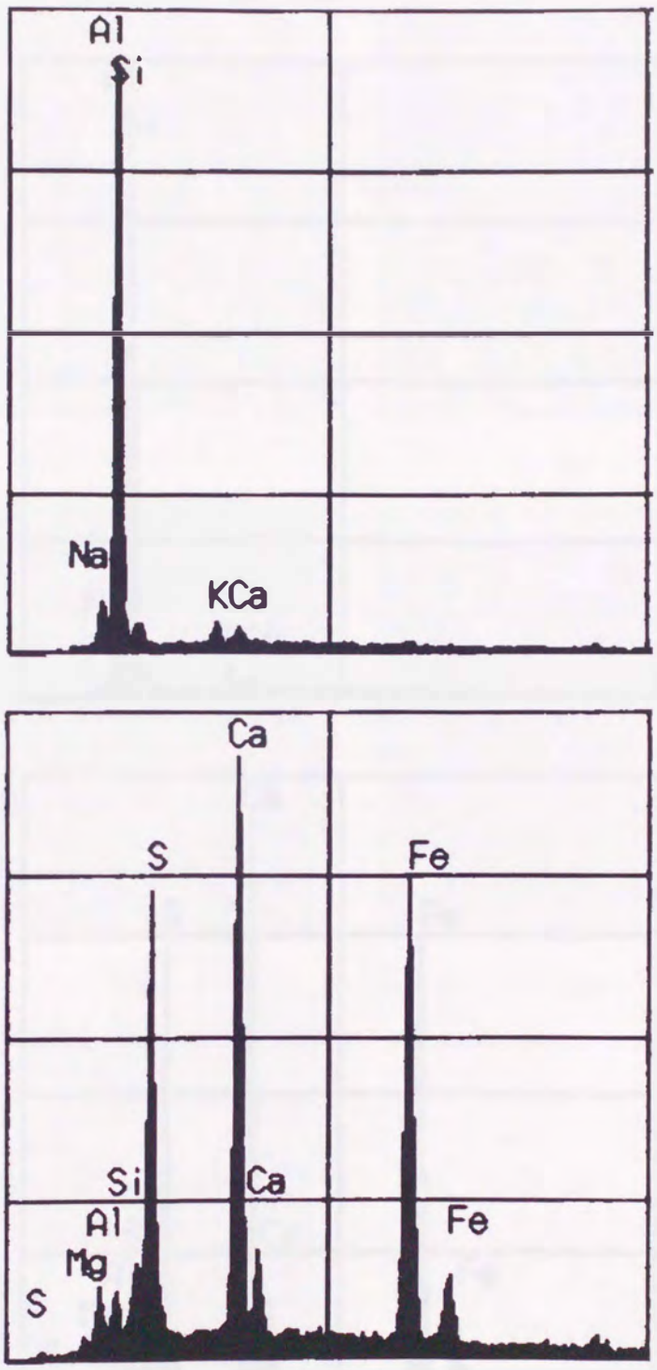

Figure 5-4. X-ray spectrometry of particles.
(a), particle #1; (b), particle #2.

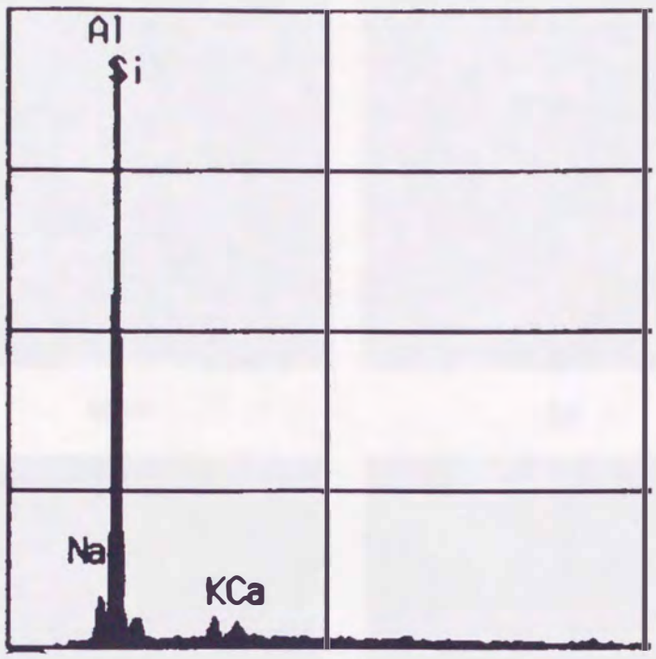

(c)

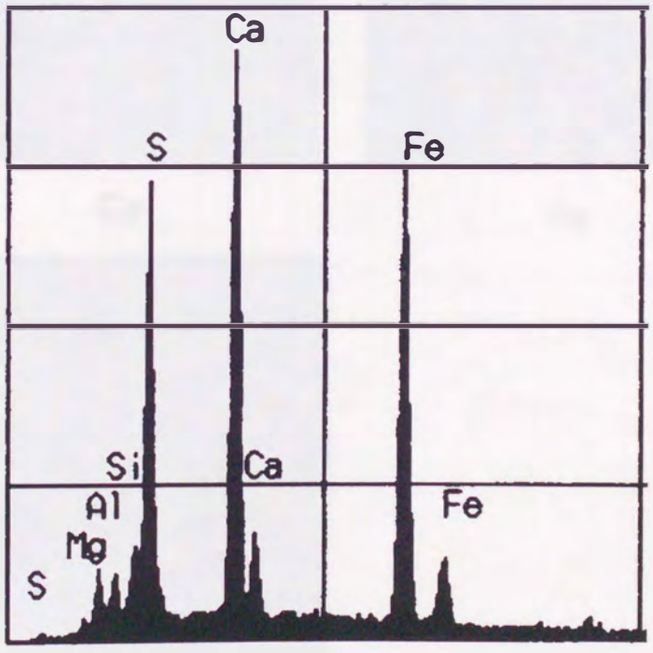

(d)

Figure 5-4. X-ray spectrometry of particles.
(c), core of particle #3;
(d), peripheral area of particle #3.

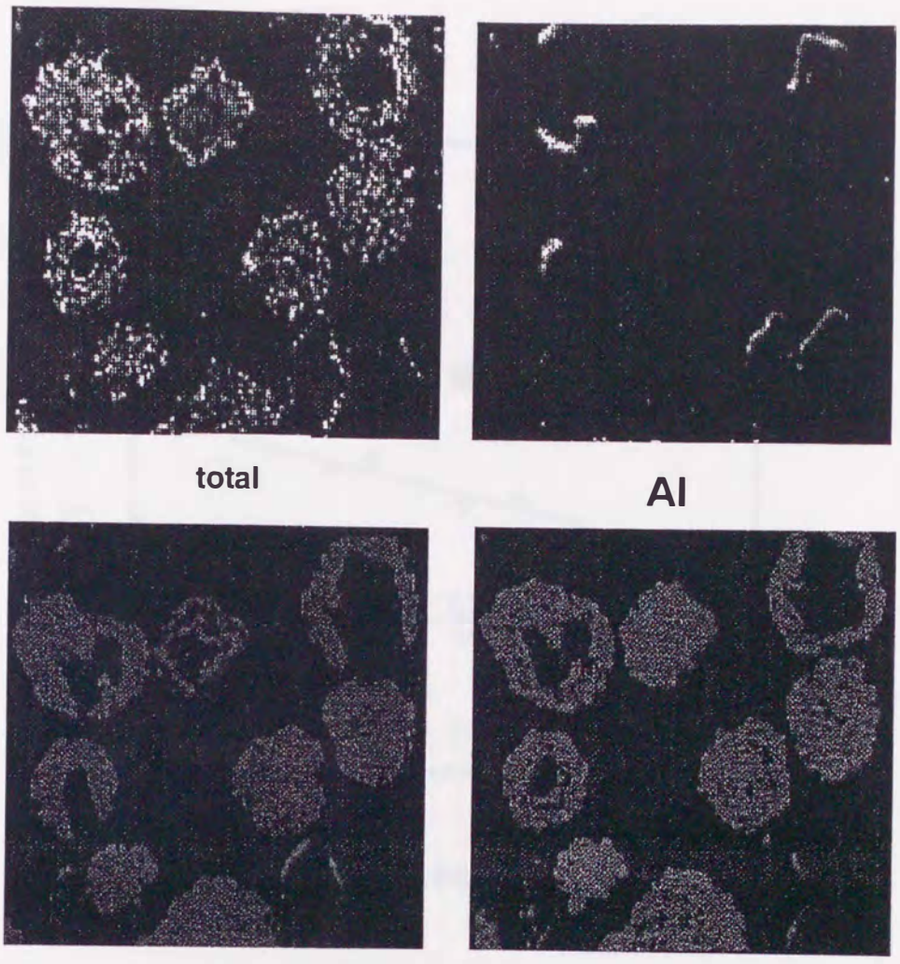

Figure 5-5. EDX images of particles.

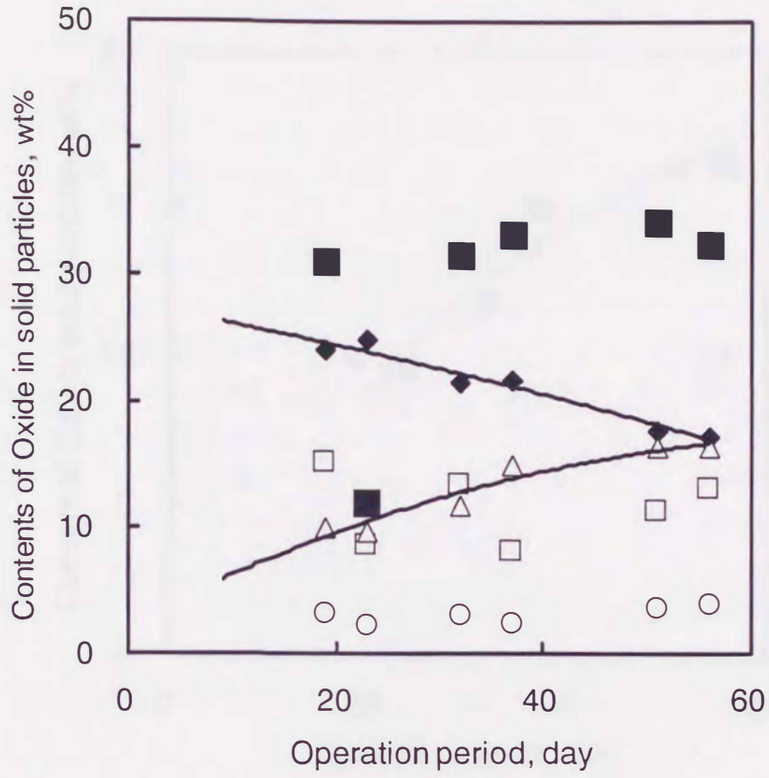

Figure 5-6. Effect of operation period on the oxide content of particles withdrawn from the bottom of the first reactor.
■, SiO_2; ◆, Fe_2O_3; □, Al_2O_3; △, CaO; ○, MgO.
Solid lines, correlations of Fe_2O_3 and CaO.

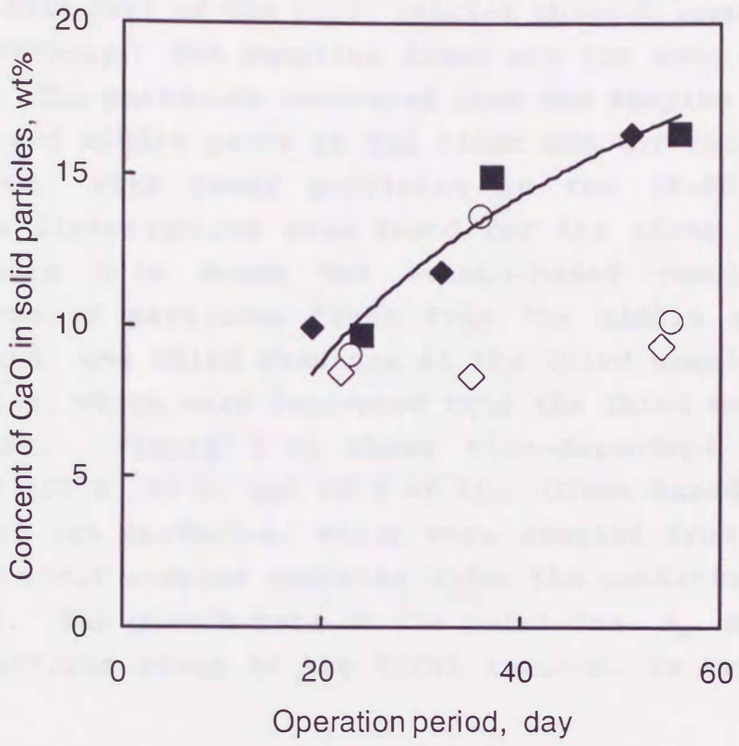

Figure 5-7. Effect of operation period on CaO content in particles.
■, from the bottom of the first reactor; ◆, from the middle of the first reactor; ○, from the middle of the second reactor; ◇, from the middle of the third reactor. Solid line, correlation from the bottom and middle of the first reactor.

Figures 5-8 and 5-9 show the volume-based cumulative size distributions of the particles, which were sampled from the bottom part of the first reactor through sampling nozzle (C) and from the middle part of the first reactor through sampling nozzle (B), respectively. The sampling times are the same as shown in Figure 5-1. The particles recovered from the samples taken from the bottom and middle parts of the first reactor show dual-peak distributions, with fewer particles in the 30-80 μm range. Smooth size distributions were found for the other particles.

Figure 5-10 shows the volume-based cumulative size distributions of particles taken from the middle part of the first, second, and third reactors at the third sampling period. The particles, which were recovered from the third reactor, were the smallest. Figure 5-11 shows time-dependent changes in diameter of 100 %, 95 %, and 90 % of the volume-based cumulative frequency of the particles, which were sampled from the bottom part of the first reactor operated under the conditions of cases 2, 3, and 4. The growth rate of the particles, K_g, based on the maximum particle sizes in the first reactor, is approximately 0.10 nm s^{-1}.

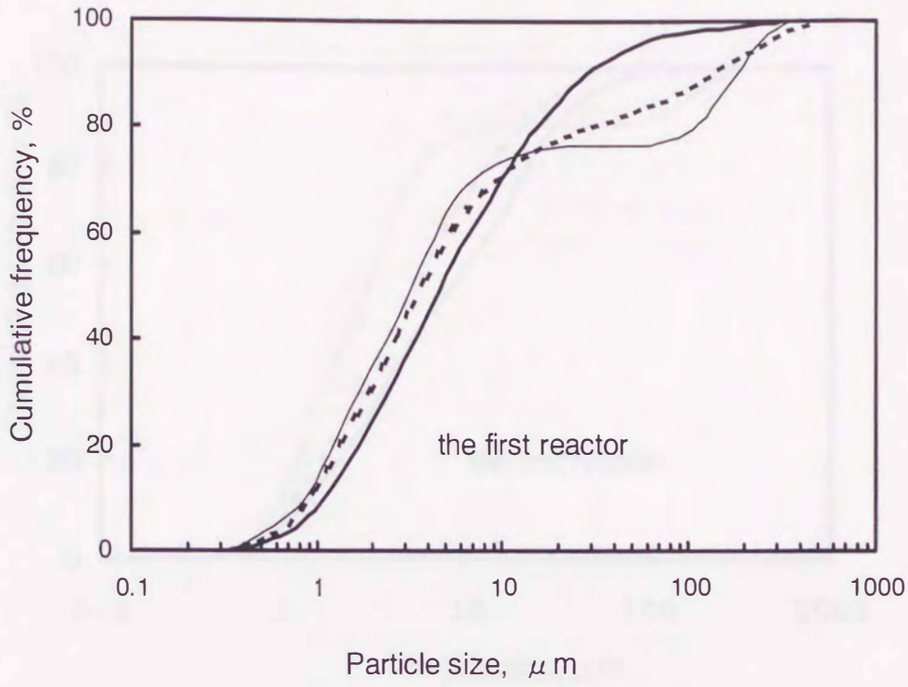

Figure 5-8. Particle size distributions of samples withdrawn from the bottom of the first reactor. Solid line, 24th day; broken line, 37th day; thin line, 56th day.

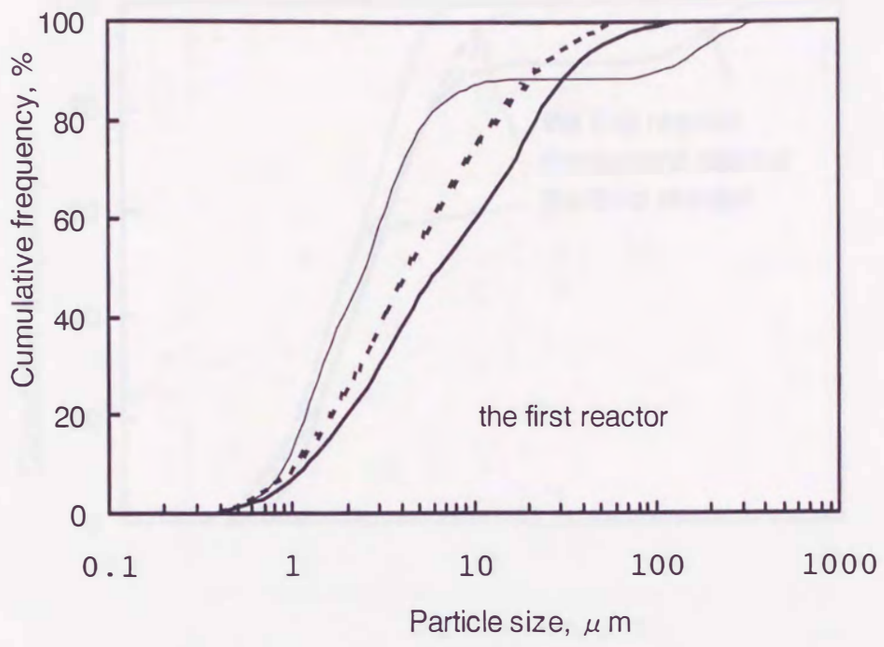

Figure 5-9. Particle size distributions of samples withdrawn from the middle of the first reactor. Solid line, 29th day; broken line, 32th day; thin line, 51th day.

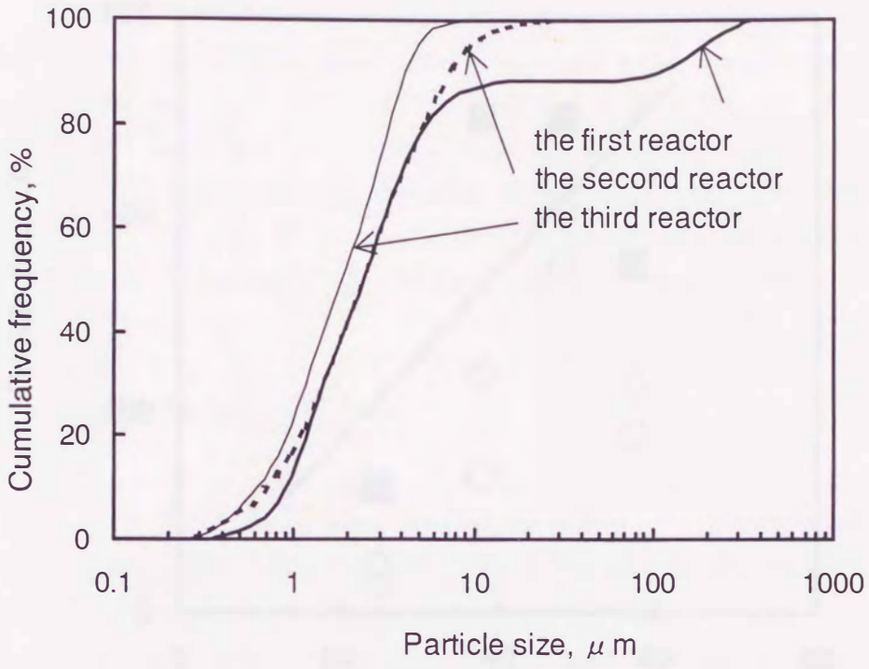

Figure 5-10. Particle size distributions of samples Withdrawn from the middle of the reactors on the 51-54th day.

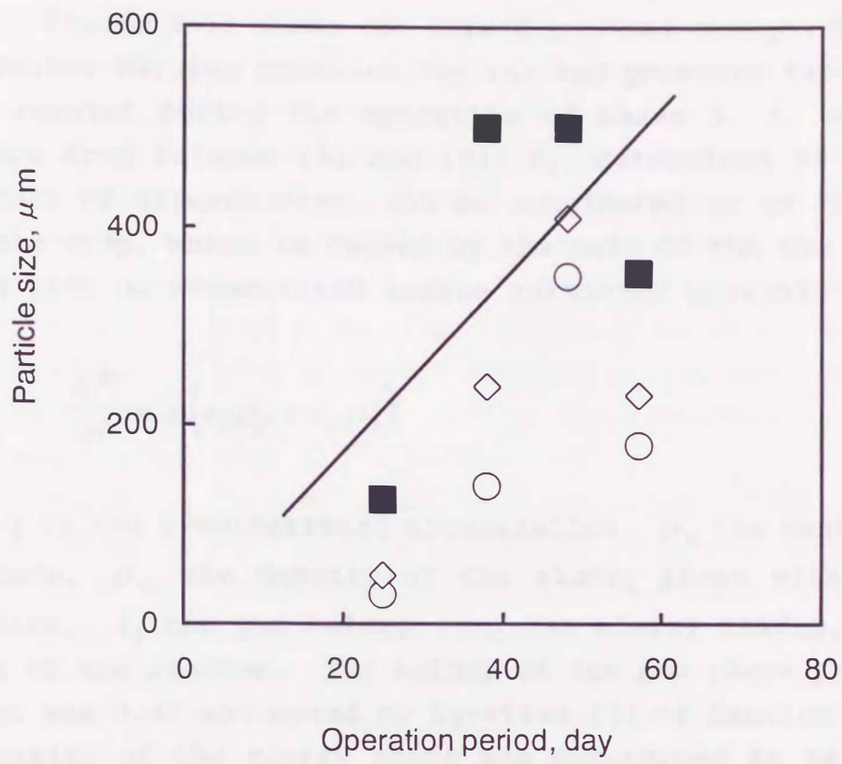

Figure 5-11. Effect of operation period on diameter of solid particles withdrawn from the bottom of the first reactor.
■, 100% of cumulative frequency; ◇, 95% of cumulative frequency; ○, 90% of cumulative frequency.
Solid line, correlation of 100% of cumulative frequency.

5.4 Pressure Drop and Accumulated Solid Particles

Figure 5-12 shows the time-dependent changes in pressure differences between pressure tap (A) and pressure tap (D) in the first reactor during the operation of cases 2, 3, and 4. The pressure drop between (A) and (D), P_d, determined at 12 h after the start of liquefaction, can be considered to be the standard pressure drop, which is caused by the mass of the gas and slurry phases with no accumulated coarse particles present.

$$\frac{\Delta P}{H} = g\left(\varepsilon_g \rho_g + \varepsilon_{sl} \rho_{sl}\right) \qquad (1)$$

where g is the gravitational acceleration, ρ_g the density of the gas phase, ρ_{sl} the density of the slurry phase without coarse particles, ε_g the gas holdup, ε_{sl} the slurry holdup, and H the height of the reactor. The holdup of the gas phase in the first reactor was 0.47 estimated by Equation (5) of Section 2.4. Thus the density of the slurry phase was determined to be 743 kg m^{-3} from the slope of the pressure difference along the reactor height. The pressure difference remained unchanged in the second and third reactors during the entire reaction period. However, the pressure difference rose gradually with operation time in the first reactor, and increased by 45 kPa after 2 months of operation. Since no severe scaling was observed on the walls of any of the reactors by visual inspection after the operation, it would appear that this increase is caused by an accumulation of coarse solid particles in the first reactor. The particle density is 2700 kg m^{-3} as described above. If the coarse particles are homogeneously suspended in the first reactor, the increase in the pressure-difference, ΔP, is given by

$$\frac{\Delta P}{H} = g\left(\varepsilon_g \rho_g + \varepsilon_{sl} \rho_{sl} + \varepsilon_s \rho_s\right) \qquad (2)$$

where ε_s and ρ_s are the holdup and density of the coarse

particles, respectively. In this report, the slurry itself consists of liquid and fine particles but does not include the coarse solid particles. The application of Equation (2) indicates that approximately 14 % and 18 % of the volume of the first reactor was occupied by accumulated coarse solid particles at the end of the operation of case 3 and case 4, respectively. Thus the concentration of the coarse particles in the mixture consisting of the slurry and the coarse particles in the first reactor is approximately 25 wt% and 34 wt% for cases 2 and 3, respectively. Based on the material balance of calcium, approximately 1.2 wt% of the calcium which had been contained in the feed coal had accumulated in the first reactor at the end of the operation of case 4.

Figure 5-13 shows the concentration of solids in the samples, which were directly withdrawn from the first reactor. In this case, the concentration is defined as the mass of solids per unit mass of the liquid-solid mixture. The mass of the liquid was calculated from the fraction having a boiling point higher than 623 K. The mass of the solids was calculated from the tetrahydrofuran (THFI) insoluble fraction or from the ash which was determined by elemental analysis. It is posible that the concentration of the solids in the liquid-solid mixture existing in the reactor is smaller than that of the THFI and larger than that of the ash. The former includes organic compounds solubilized in the reactor and insolubilized in THF, and the latter does not contain coal fragments. The concentration of the solids increased with increasing operation period, and the concentration in the samples withdrawn through the nozzles (C) was higher than that in the samples withdrawn through the nozzle (B). Thus, the solid particles were accumulating in the lower part, as well as in the middle part, of the reactor after 30 days. The axial distributions of solid particles will be discussed in Chapter 6.

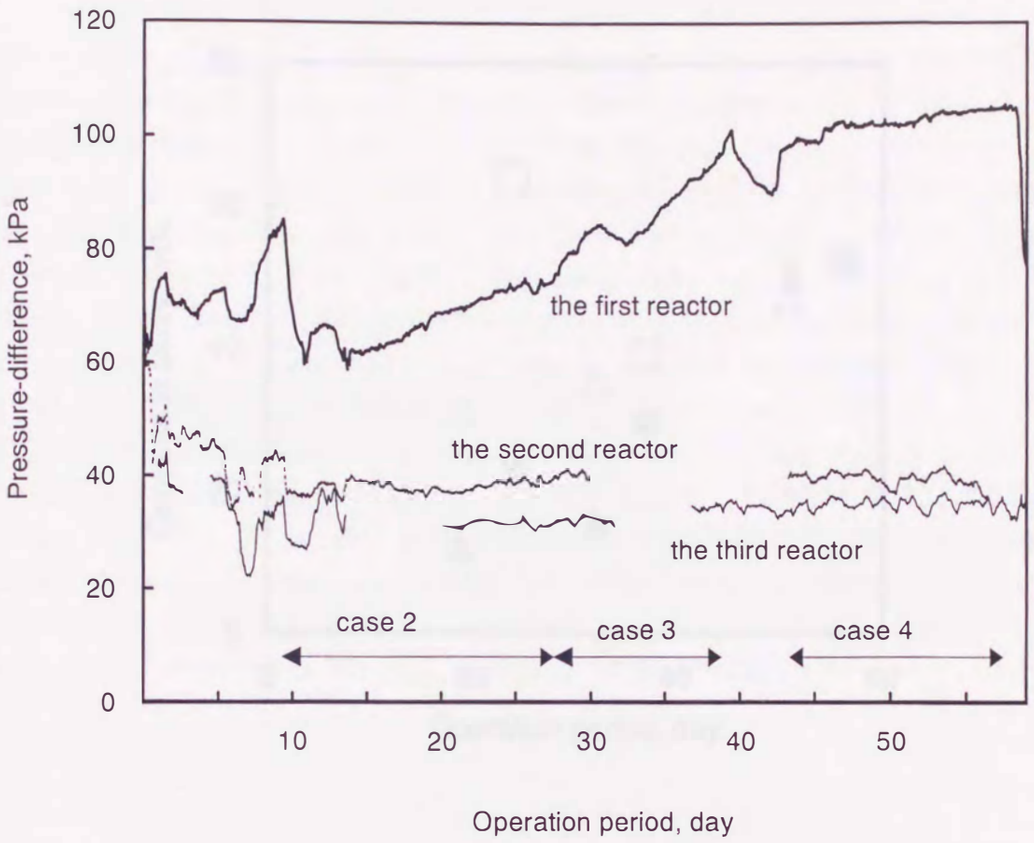

Figure 5-12. Changes in pressure differences in the reactors.

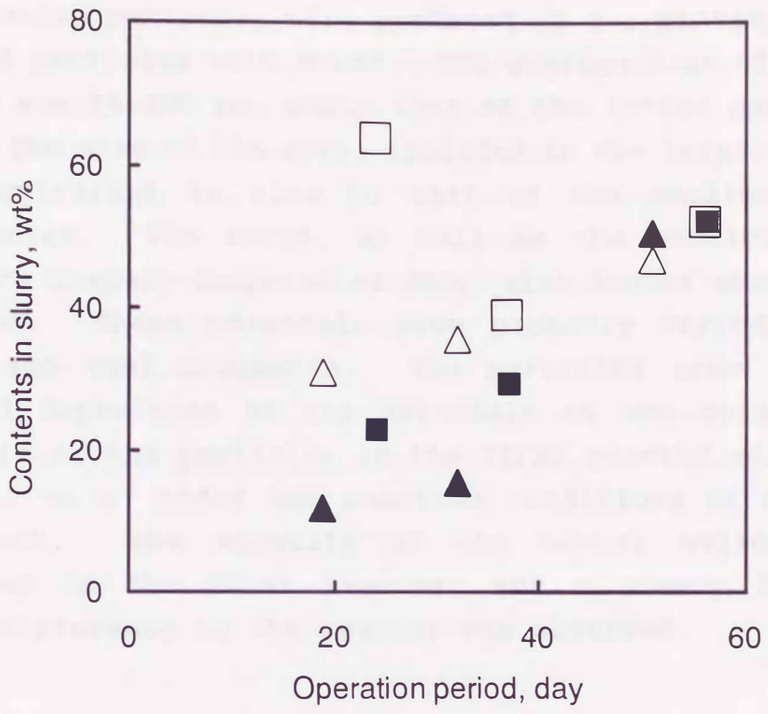

Figure 5-13. Solid concentrations in samples withdrawn from the bottom (□,■) and middle (△,▲) of the first reactor. The open and closed keys indicate the THFI and ash components, respectively.

5.5 Conclusions

During the operation of the Kashima pilot plant, two types of solid particles were produced, i.e., particles without cores, and particles with cores. The average size of the former particles was 10-200 μm, while that of the latter particles was 1-80 μm. The size of the core, included in the larger particles, was as equivalent in size to that of the smaller particles without cores. The cores, as well as the particles without cores, were largely composed of SiO_2, with lesser amounts of FeS and carbon. These materials were probably formed from ash, catalyst and coal fragments. The particles grew in size by additional deposition of the materials on the cores, and the growth rate of the particles in the first reactor was estimated to be 0.10 nm s^{-1} under the reaction conditions of the Kashima pilot plant. The majority of the coarse solid particles accumulated in the first reactor, and a steady increase in pressure difference in the reactor was observed.

Nomenclature

G_q = volumetric flow rate of quench gas, m^3(STP) s^{-1}

G_r = volumetric flow rate of recycle gas, excluding gas and oil vapor which are evolved by reactions, m^3(STP) s^{-1}

K_g = growth rate of a particle, nm s^{-1}

L_f = mass flow rate of makeup slurry, kg s^{-1}

H = effective length based on volume including top and bottom parts, m

ε_g, ε_{sl}, ε_s = volume fraction of gas including oil vapor, of slurry including fine particles, and of coarse particles

ΔP = pressure difference, kPa

ρ_g, ρ_{sl}, ρ_s = density of gas including oil vapor, of slurry including fine particles, and of coarse particles, kg m^{-3}

References

(1) Ueda, S.; Aramaki, T.; Kobayashi, M. Study on solid deposit appeared in hot high pressure separator in coal liquefaction 150t/d pilot plant. *1999 Intern. Conf. Coal Sci., Taiyuan, Shanxi*, **1999**.

(2) Aramaki, T.; Namiki, Y.; Onozaki, M.; Takagi, T.; Ueda, S.; Kobayashi, M.; Mochida, I. Solid deposit found in 150t/d pilot plant of coal liquefaction (III), minerals found in the reactors and their roles in the precipitation of minerals in the downstream unit. *J. Japan Inst. Energy* **2000**, in press.

(3) Aramaki, T.; Onozaki, M.; Takagi, T.; Kamada, M.; Ueda, S.; Kobayashi, M.; Mochida, I. Solid deposit found in 150 t/d Pilot Plant of coal liquefaction, Solid deposit in hot high pressure separator (I). *J. Japan Inst. Energy* **1999**, *78*, 929-942.

(4) Wakeley, L. D.; Davis, A.; Jenkins, R. G.; Mitchell, G. D.; Walker, P. L, Jr. The nature of solids accumulated during solvent refining of coal. *Fuel* **1979**, *58*, 379-385.

(5) Okuma, O.; Yanai, S.; Yasumuro, M.; Makino, E. Scales and sediments formed during liquefaction of Victorian brown coal with a 50 ton (dry coal)/day pilot plant. *J. Japan Inst. Energy* **1999**, *78*, 332-344.

(6) Mochizuki, M.; Imada, K.; Inokuchi, K.; Nogami, Y. Operational analysis and development of coal liquefaction 1 t/d process supporting unit. *J. Japan Inst. Energy* **1997**, *76*, 1074-1083.

(7) Onozaki, M.; Namiki, Y.; Aramaki, T.; Takagi, T.; Kobayashi, M.; Morooka, S. A simulation of the accumulation of solid particles in coal liquefaction reactors based on the NEDOL process. *Ind. Eng. Chem. Res.* **1999**, submitted.

6. A Simulation of the Accumulation of Solid Particles in Coal Liquefaction Reactors. 2. Hydrodynamics of Three-Phase Mixtures

6.1 Introduction

During liquefaction, the pressure drop between the top and bottom of the first reactor gradually increased as the operation time passed. Samples which were taken directly from the reactors contained solid particles of a few to 500 μm in diameter. The concentration of solids at the bottom of the first reactor was higher than that at the middle and top of the reactor. This suggests that the holdup of solid particles was axially distributed in the reactor. Ueda et al.[1] and Aramaki and the author et al.[2,3] reported that grown particles recovered from the Kashima pilot plant were composed of the cores containing SiO_2, FeS and Al_2O_3 and the peripherals containing $CaCO_3$, FeS, and $MgCO_3$. These particles are comparable to those found in the SRC plant in Wilsonville[4], the BCL plant in Victoria[5], and the process supporting unit (PSU) in Kimitsu[6].

Morooka et al.[7] discussed the hydrodynamics of particle sedimentation in liquefaction reactors, based on balances among entrainment, growth, and axial dispersion of solid particles. However, the theory was not validated with experimental data obtained in actual liquefaction reactors. The objective of the present study[8] is to evaluate the solid accumulation, based on the data of the Kashima pilot plant.

6.2 Pilot Plant Operation and Accumulated Solid Particles

As shown in Figure 5-11, the pressure difference along the length of the first reactor was increased by 45 kPa during the operation for two months. The pressure difference did not change immediately after the startup. However, it increased by 1.3 kPa per day after 14 days passed. When fine solid particles are completely suspended in the liquid phase, the pressure difference per unit reactor length, $\Delta P/H$, is given as follows:

$$\frac{\Delta P}{H} = \left(\varepsilon_g \rho_g + \varepsilon_{sl} \rho_{sl}\right) g \qquad (1)$$

where ε_g and ε_{sl} are the volume fractions of gas and slurry per unit volume of the reactor, respectively. ρ_g and ρ_{sl} are the densities of gas and slurry, respectively. Immediately after the startup of liquefaction, most particles are less than 10 μm. The terminal velocity of a particle with a diameter of 10 μm is approximately 0.0002 m s^{-1}, which is much smaller than the superficial liquid velocity in the reactor (typically 0.0038 m s^{-1}). Thus the slurry phase is assumed to be a homogeneous pseudo-liquid. However, larger particles appeared in the lower part of the reactor after a long liquefaction period. Samples, which were removed from the bottom of the first reactor, showed that solid particles occupied a volume fraction of 0.2-0.4 in the liquid-solid mixture, as reported in Section 5.4. The volume fraction of fine solid particles in the slurry phase, which was sampled from the higher part of the reactor, was calculated to be 0.09, as described in Section 5.4. This suggests that coarse particles existed in the state of a fluidized bed in the lower part of the first reactor. In that case, the pressure difference, $\Delta P/H$, is described as follows:

$$\frac{\Delta P}{H} = \left(\varepsilon_g \rho_g + \varepsilon_{sl} \rho_{sl} + \varepsilon_s \rho_s\right) g \qquad (2)$$

where ε_s is the volume fraction of coarse solid particles per unit volume of the reactor (hereafter referred to as solid

holdup), and ρ_s is the density of coarse solid particles.

As reported by Aramaki and the author et al.[2] and Onozaki et al.[8], solid particles which accumulated in the reactors were classified to coarse particles with a core and fine particles without a core. The cores consisted of SiO_2, FeS and Al_2O_3, and the peripherals consisted of $CaCO_3$, FeS, and $MgCO_3$. Particles without cores contained SiO_2, FeS and Al_2O_3, and were similar to the cores. Although solid particles are not always spherical, they are assumed to be spherical in the present study. Since the average size of the cores is approximately 25 μm, the particles with the diameter larger than 25μm are hereafter referred to as the coarse solid particles. The solid particles, which are smaller than 25 μm, are, as a definition, included in the slurry phase. The average density of the solid particles was determined to be 2700 kg m^{-3}. The growth rate of particles based on the volume-based size distribution, K_g, was found to be 0.10 nm s^{-1} as described in Section 5.3.

6.3 Modeling of Solid Accumulation

Figure 6-1 shows a model describing the axial concentration distribution of coarse solid particles in the first reactor. The reactor is assumed to consist of two regions, a dense region at the lower part and a lean region at the upper part. The fine particles without cores are included in the slurry phase, and most of them are carried out along with the ascending liquid flow. However, some particles remain in the reactor as a result of the axial dispersion, and grow to coarse particles, which cannot be entrained by the liquid flow. A portion of the coarse particles can be discharged from the reactor also by the axial dispersion.

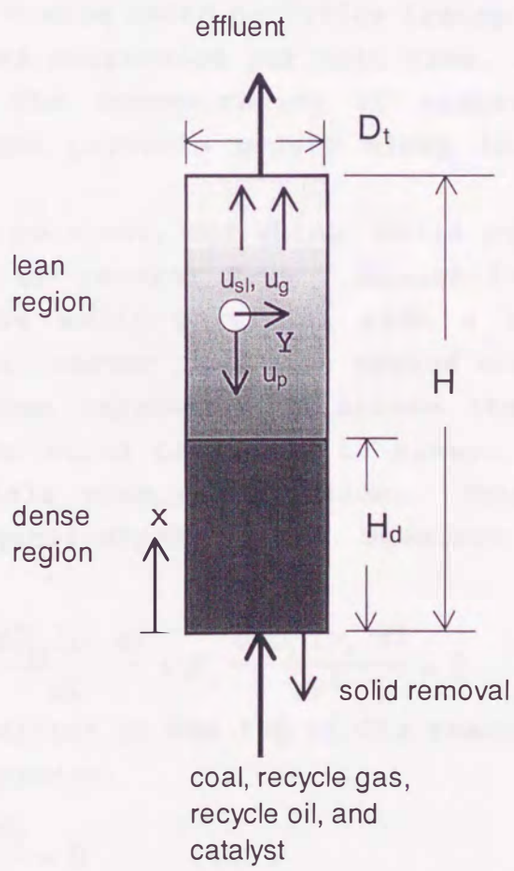

Figure 6-1. A model of the first reactor.

Upper Lean Region

A one-dimensional sedimentation-dispersion model is applied to the lean region. The population balance of coarse solid particles proposed by Morooka et al.[7] is described as follows:

$$-\frac{\partial C_L(y,x,t)}{\partial t}+\left(U_p-U\right)\frac{\partial C_L(y,x,t)}{\partial x}+E_p\frac{\partial^2 C_L(y,x,t)}{\partial x^2}-\frac{\partial}{\partial y}\left\{\kappa_g C_L(y,x,t)\right\}=0 \qquad (3)$$

where $C_L(y,x,t)$ is the concentration of coarse solid particles, t the time, x the axial height of the reactor, y the coordinate of the particle size, U the linear velocity of the slurry, U_p the sedimentation velocity of coarse particles, E_p the axial dispersion coefficient of coarse solid particles. The second and third terms on the left-hand side of Equation (3) are the concentration of coarse solid particles transported by the liquid flow and the axial dispersion per unit time, respectively. The fourth term is the concentration of coarse solid particles transferred by the particle growth along the y-axis per unit time.

The time constant, for which solid particles are grown, is of the order of several days. Meanwhile, a concentration profile of coarse solid particles with a size of y_n can be stabilized in the reactor in a time period shorter than several hours. It is then reasonable to assume that a concentration profile of coarse solid particles is always established for a prescribed particle size distribution. Thus Equation (3) is reduced to a quasi-steady state equation for $C_{Lt}(y_n,x)$ as follows:

$$\left(U_p-U\right)\frac{dC_{L_t}(y_n,x)}{dx}+E_p\frac{d^2C_{L_t}(y_n,x)}{dx^2}=0 \qquad (4)$$

The boundary condition at the top of the reactor is described by the following equation.

$$\frac{dC_{L_t}(y_n,H)}{dx}=0 \qquad (5)$$

Thus the concentration of coarse particles with a diameter of y_n at a height of x is given as

$$C_{Lt}(y_n, x) = C_{Ft}(y_n)\left[\frac{U_p}{U_p - U}\exp\left\{\frac{U_p - U}{E_p}(H - x)\right\} - \frac{U}{U_p - U}\right] \qquad (6)$$

where $C_{Ft}(y_n)$ is the concentration of coarse particles with a diameter of y_n in the feed stream at the inlet nozzle. The amount of the coarse particles with a diameter of y_n in the reactor, $W_{Lt}(y_n)$, is obtained by integrating $C_{Lt}(y_n,x)$ over the range of x = 0 - H.

$$W_{Lt}(y_n) = \int_0^H C_{Lt}(y_n, x)dx \qquad (7)$$

where H is the height of the reactor.

$W_{Lt}(y_n)$ is increased to $W_{Lt}(y_{n+1})$ by a factor of $(y_{n+1}/y_n)^3$ if no coarse particles are entrained to the outside by the liquid flow. Actually, however, the mass of the coarse particles, which are carried out due to the entrainment, should be subtracted from $W_{Lt}(y_{n+1})$.

$$W_{Lt}(y_{n+1}) = \left\{W_{Lt}(y_n) - \left(\frac{C_{Lt}(y_n, H) + C_{Lt}(y_{n+1}, H)}{2}\right)F_T\right\}\left(\frac{y_{n+1}}{y_n}\right)^3 \qquad (8)$$

where F_T is the flow rate of the effluent slurry causing the entrainment. $C_{Lt}(y_n,x)$ can be calculated from Equations (6)-(8).

The feed concentration of core particles, $C_{Ft}(y_0)$ is related to the concentrations of ash and catalyst and is assumed to be constant in the present simulation.

$$C_{Ft}(y_0) = constant \qquad (9)$$

where y_0 is the diameter of the core particle. The core particles grow at a rate K_g, which is assumed to be independent of particle size. Thus, y_{n+1} and y_n are connected by the following equation.

$$y_{n+1} = y_n + K_g\Delta t \qquad (10)$$

where Δt is the time interval in which y_n increases to y_{n+1} at a linear growth rate K_g.

The total concentration of particles at x, $S_L(x,t)$, is then calculated by integrating $C_{Lt}(y_n,x)$ over the particle size, y.

$$S_L(x,t) = \int_{y_0}^{y_e} C_{L_t}(y,x)dy \qquad (11)$$

where y_e is the maximum diameter at t. y_0 is assumed to be 25 μm in the present case.

Lower Dense Region

When the liquefaction starts, only core particles exist in the reactor. As the operation continues, coarse particles are concentrated at the bottom. The behavior of the coarse particles in the lean region above the dense region is described by the sedimentation dispersion model, as expressed in the preceding section. When the concentration of coarse particles exceeds a threshold value, however, a condensed zone of coarse particles appears in the lower region. This region is hereafter referred to as the dense region. Kato et al. [10] (1985) reported that the threshold of the solid holdup, defined for coarse particles, in the dense region was approximately 0.5. In the present study, however, the threshold value of the solid holdup is decided to be 0.4, since fine particles which are homogeneously suspended in the slurry phase may increase the drag force. The height of the dense region is assumed to be equal for all solid particles with cores, irrespective to their particle diameters. The threshold concentration, S_{max}, is related to the solid holdup in the dense region, ε_{sd}, which is constant with respect to the axial position.

$$S_{max} = \varepsilon_{sD}\rho_s \qquad (12)$$

When the total concentration of particles at the bottom, $S_L(0,t)$ is more than S_{max}, a dense region is formed. It can be assumed that solid concentration, a function of operation period, t, in a fluidized bed, $C_D(y,t)$ is independent of the axial position. The mass of grown particles having a diameter of y_n in the dense region, $W_D(y_n,t)$, is then calculated from

$$W_D(y_n,t) = C_D(y_n,t)H_d(t) \qquad (13)$$

where H_d is the height of the dense region. In the lean region, the solid concentration is calculated from the following equation

as a function of operation period t.

$$C_L(y_n,x,t) = C_F(y_n,t)\left[\frac{U_p}{U_p - U}\exp\left\{\frac{U_p - U}{E_p}(H - x)\right\} - \frac{U}{U_p - U}\right]$$

$$H_d(t) \le x \le H \qquad (14)$$

where H_d is the height of the dense region. The boundary condition between the lean and dense regions is expressed by

$$C_L(y_n,H_d,t) = C_D(y_n,H_d,t)\,. \qquad (15)$$

Assuming $C_F(y_n,t)$ and H_d, $W(y_n,t)$ is calculated by the following euqation, using Equations (14) and (15).

$$W(y_n,t) = W_D(y_n,t) + W_L(y_n,t)$$
$$= C_D(y_n,t)H_d(t) + \int_{H_d}^{H} C_{L_t}(y_n,x,t)dx. \qquad (16)$$

The mass of particles having a diameter y_n at t_m, $W(y_n,t_m)$, is related to the state at t_{m-1} by the following equation.

$$W(y_n,t_m) = \left\{W(y_{n-1},t_{m-1}) - \left(\frac{C_L(y_{n-1},H,t_{m-1}) + C_L(y_n,H,t_{m-1})}{2}\right)F_T\right\}\left(\frac{y_n}{y_{n-1}}\right)^3 \qquad (17)$$

$C_F(y_n,t)$ is determined by the successive calculations from the state with only the lean region to the state with the two regions with Equations (14) to (17). After the dense region appears, $H_d(t)$ is determined each time so as to satisfy Equations (12) and (13).

The pressure difference along the reactor length, P_d, is calculated from

$$\frac{\Delta P}{H} = \int_{y_i}^{y_e} W_t(y)g\,dy \qquad (18)$$

If the gas-liquid-solid mixture is removed from the dense region at a flow rate of F_R, Equation (17) is modified to the following equation.

$$W(y_n,t_m) = \left\{W(y_{n-1},t_{m-1}) - \left(\frac{C_L(y_{n-1},H,t_{m-1}) + C_L(y_n,H,t_{m-1})}{2}\right)F_T - \left(\frac{C\,(y_{n-1},H_R,t_{m-1}) + C\,(y_n,H_R,t_{m-1})}{2}\right)F_R\right\}\left(\frac{y_n}{y_{n-1}}\right)^3 \quad (19)$$

where suffix R means the axial position of the removal nozzle. $C(y_{n-1},H_R,t_{m-1})$ is the concentration of coarse particles in the removal flow. Usually, the removal of the mixture is undertaken near the bottom of the first reactor. This means that $C(y_{n-1},H_R,t_{m-1})$ is equal to $C_D(y_{n-1},H_R,t_{m-1})$ with the two regions.

6.4 Estimation of Parameters Used in the Model

6.4.1 Operating Conditions

In the present study, "standard operation" (case 2) of Tanitoharum coal was principally adopted for simulation as shown in Table 3-1.

6.4.2 Gas Holdup

Equation (5) in Section 3.4 was used in the present study to predict gas holdup.

6.4.3 Axial Dispersion Coefficient

At the Kashima pilot plant, Sakai and the author et al.[10] used a neutron absorption tracer technique and determined E_l = 0.018 and 0.029 $m^2\ s^{-1}$ at U_g = 0.058 and 0.056 m s^{-1}, respectively as shown in Table 2-8. These values can be correlated using the following equation which is derived by modifying Equation (6) of Section 2.5.

$$E_l = f_D U_g^{0.3} \qquad (20)$$

where f_D is 0.042 and 0.069 for U_g = 0.058 and 0.056 m s^{-1}, respectively, and the average value is 0.056. Hidaka et al.[11] reported that the axial dispersion coefficient of solid particles, which were fluidized in the dense region (particle diameter, 2.2, 3.1 and 4.65 mm), were 0.9 times that of the liquid. In order to simplify the computation, E_l, which is calculated from Equation (20) using f_d = 0.056, is adopted for E_p of Equations (4), (6) and (14).

6.4.4 Physical Properties of Gas and Slurry

The flow rates of the gas and liquid in the reactors were estimated using the simulator as shown in Section 2.3. Adding the solid properties to Table 2-6, model parameters are shown in Table 6-1.

Table 6-1. Model parameters and simulation conditions for case 2

Gas Phase	
Density, kg m^{-3}	48
Calculated superficial velocity, m s^{-1}	0.056
Liquid Phase	
Density of liquid, kg m^{-3}	670
Viscosity of liquid, kg m^{-1} s^{-1}	0.0007
Calculated superficial velocity, m s^{-1}	0.0038
Solid Particle	
Density, kg m^{-3}	2700
Initial diameter of particle, μm	25
Conversion ratio from ash and catalyst of feed slurry to cores, wt%	10
Growth rate of particles, nm s^{-1}	0.10
Calculated gas holdup	0.47
Calculated axial dispersion coefficient, m^2 s^{-1}	0.024
Maximum solid holdup	0.4

6.4.5 Sedimentation Velocity

Kato et al. [12] measured the mean settling velocity of solid particles, which were suspended in bubble columns. The particles were glass spheres, the average diameters of which were 74-162 μm. Their data are correlated as

$$U_p = 1.33 U_l \left(\frac{U_g}{U_t} \right)^{0.25} Q^{2.5} \qquad (21)$$

where

$$Q = \frac{\varepsilon_l}{\varepsilon_l + \varepsilon_s} \qquad (22)$$

Kato et al. [9] extended the above correlation to the lean region of the three-phase fluidized bed and proposed the following correlation.

$$U_p = U_l \left\{ 1 + 1.5 \left(\frac{U_g}{U_t} \right) \right\}^{0.30} Q^{2.5} \qquad (23)$$

where u_t is the terminal velocity of an isolated solid particle. However, the drag coefficient of particles highly depends on particle shapes and flow properties. Thus the terminal velocity of an isolated particle in the reactors of the Kashima pilot plant is determined by the following equation.

$$U_t = K_p y^2 \left(\rho_p - \rho_l \right) g \, / \, 18 \mu_l \qquad (24)$$

Since the holdup of coarse particles is much smaller than the liquid holdup in the lean region, Q in Equation (23) is assumed to be unity. U_p is calculated from Equations (24), where K_p is used as an adjustable parameter in the present calculation.

6.5 Results

The pressure difference between the pressure taps (A) and (D) was calculated for case 2 as a typical condition. Table 6-1 shows the data, as well as estimated values, used for the simulation for case 2. When 10 wt% of ash and catalysts in the feed slurry were converted to the core particles, the calculated pressure drop was coincident with the measured value. The concentration of the core particles fed to the reactor, $C_{Ft}(y_0)$, was estimated by this ratio. Figure 6-2 shows the time-dependent changes in the pressure difference along the reactor length, as a function of K_p defined by Equation (24). The calculation is closest to the data when K_p is assumed to 2.5. When K_p is increased to 2.8, the pressure difference starts to increase too early. When K_p is reduced to 1.0, on the other hand, the pressure difference increases too slowly.

Once the dense region appears, the height of the dense region increases rapidly, as shown in Figure 6-3. The estimated concentration profiles on the 9th and 25th days from the start are shown in Figures 6-4 and 6-5. No dense region exists on the 9th day. As shown in Figures 6-5, however, the height of the dense region reaches approximately 20 % of the reactor height. Figure 6-6 (a) shows the particle size distributions which were obtained for the samples recovered at the middle of the first reactor on the 19th and 51st days from the start. These data are well in agreement with the calculation, as shown in Figure 6-6 (b), where the estimated weight-based distributions are transformed to the number-based distributions. Particles less than 25 μm in diameter are added to the calculated distribution in Figure 6-6 (b), in order to compare them with the experimental distributions. Experimental distributions are broader than the calculated distributions due to a variety of sizes of core particles. As the time proceeds, the particles between 30 and 80 μm in diameter are entrained, and most of them disappear on the 51th day.

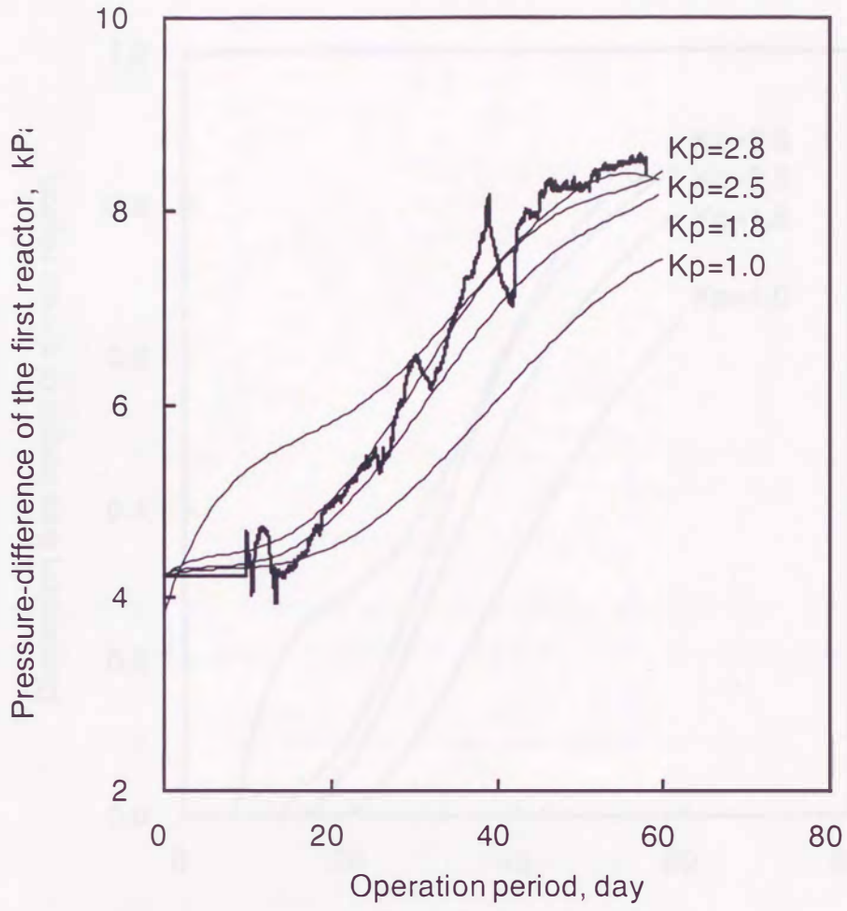

Figure 6-2. Pressure difference in the first reactor.
Solid line, experiment; thin line, calculation.

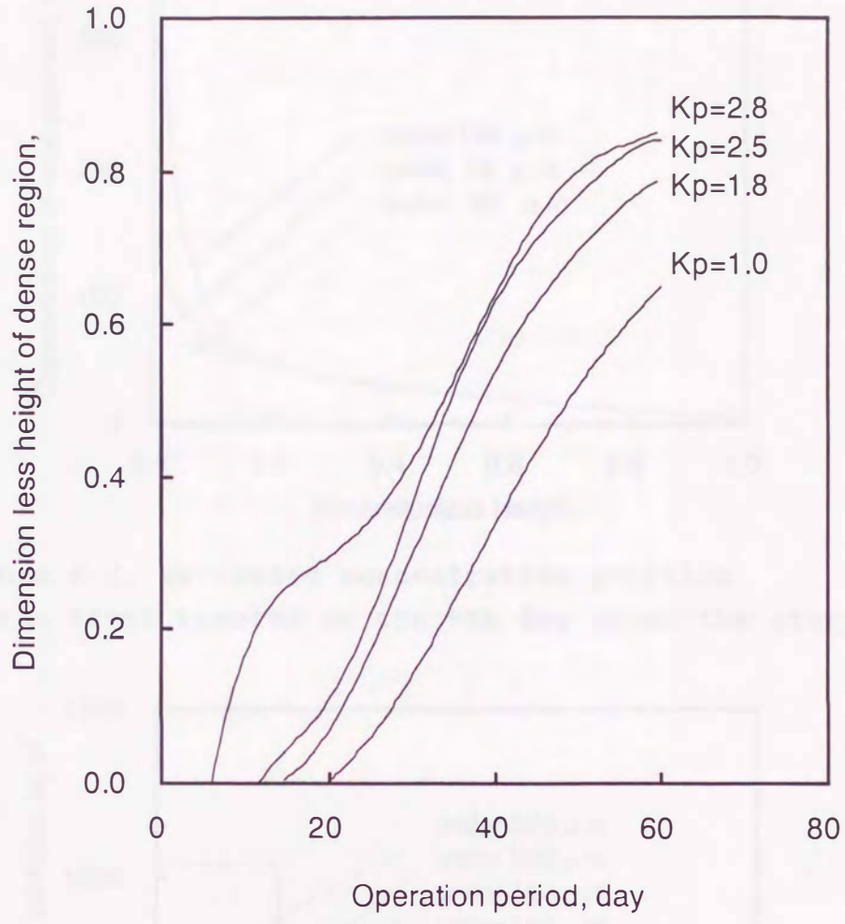

Figure 6-3. Estimated dimensionless heights of dense region in the first reactor.

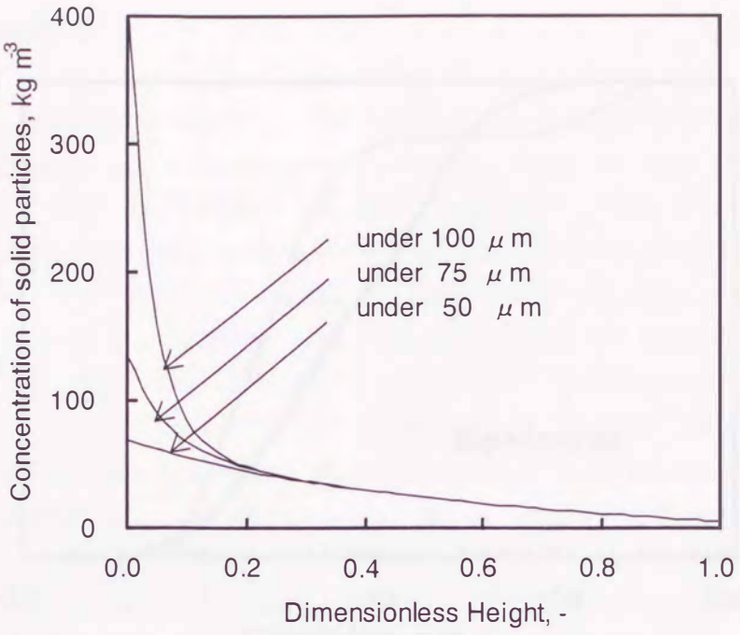

Figure 6-4. Estimated concentration profiles
in the first reactor on the 9th day after the startup.

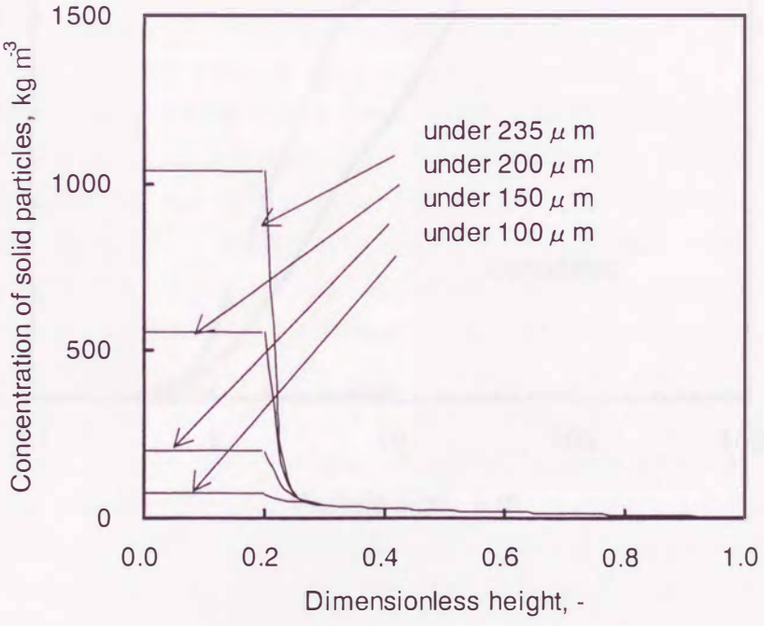

Figure 6-5. Estimated concentration profiles
in the first reactor on the 25th day after the startup.

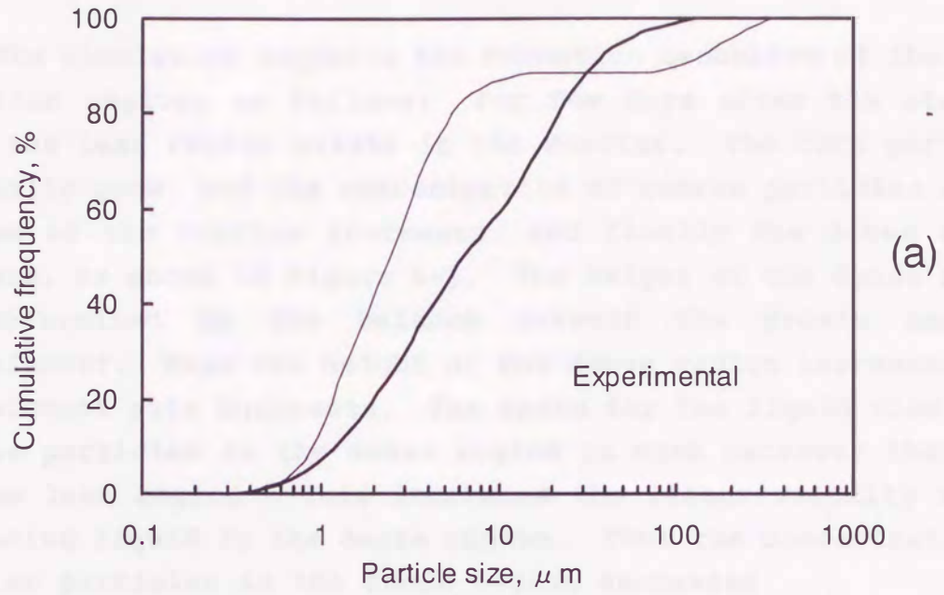

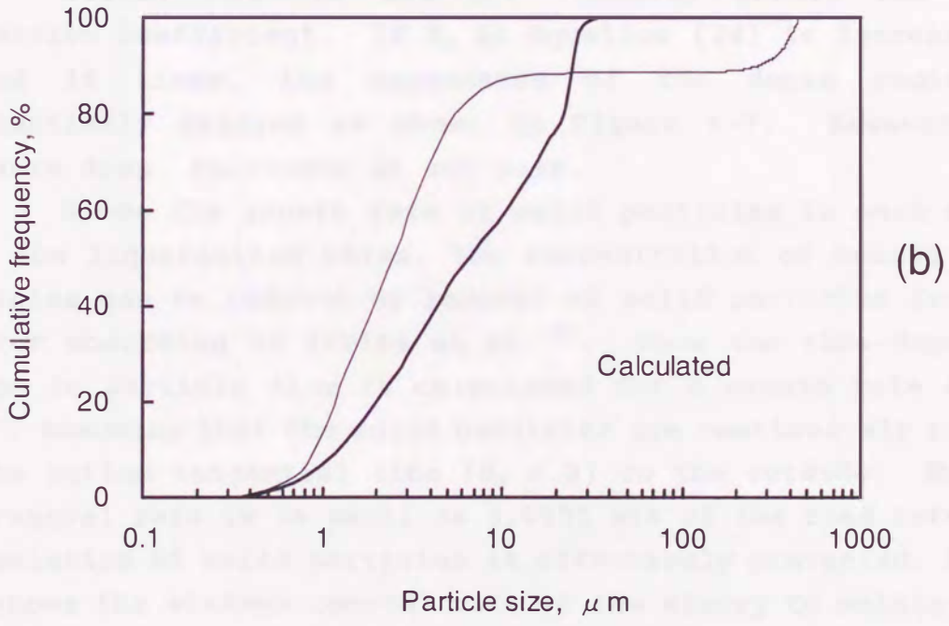

Figure 6-6. Estimated particle size distributions at the middle of the first reactor.
(a), experiment; (b), calculation.
Solid line, on the 19th day; thin line, on the 51th day.

6.6 Discussion

The simulation suggests the formation mechanism of the dense and lean regions as follows: For few days after the startup, only the lean region exists in the reactor. The core particles gradually grow, and the concentration of coarse particles at the bottom of the reactor increases, and finally the dense region appears, as shown in Figure 6-1. The height of the dense region is determined by the balance between the growth and the entrainment. When the height of the dense region increases, the entrainment rate increases. The space for the liquid flow among coarse particles in the dense region is much narrower than that in the lean region. This increases the linear velocity of the ascending liquid in the dense region. Thus the concentration of smaller particles in the dense region decreases.

Column diameter and gas velocity affect the axial dispersion coefficient. If K_d in Equation (24) is increased by 4 and 16 times, the appearance of the dense region is substantially delayed as shown in Figure 6-7. However, the pressure drop increases in any case.

Since the growth rate of solid particles is much slower than the liquefaction rates, the concentration of coarse solid particles can be reduced by removal of solid particles from the reactor according to Irvine et al.[13]. Thus the time-dependent change in particle size is calculated for a growth rate of 0.1 nm s^{-1}, assuming that the solid particles are continuously removed at the bottom tangential line (H_R = 0) to the outside. Even if the removal rate is as small as 0.0055 wt% of the feed rate, the accumulation of solid particles is effectively prevented. Figure 6-8 shows the minimum removal rate of the slurry to maintain the pressure difference at the same level. For a growth rate of 0.20 nm s^{-1}, the solid accumulation can be avoided, when 0.06 wt% of the feed slurry is removed from the bottom of the reactor. As Okuma et al.[5] reported, the accumulation of solid particles may suppress the scaling on the reactor walls, since precursors of the scaling are deposited as particles. In order to prevent both the scaling on the reactor walls and the accumulation of coarse

particles, the removing rate from the reactor bottom should be carefully adjusted. The hydrodynamic model for the solid accumulation, proposed in this study, is effective for this decision.

In the present study, it is assumed that coarse particles are homogeneously fluidized in the dense bed. However, Hidaka et al.[11] and Matsumoto et al.[14] analyzed concentration profiles of coarse particles in the dense region for multi-component systems, and found that there were some separations of particles. This problem is left for a future study.

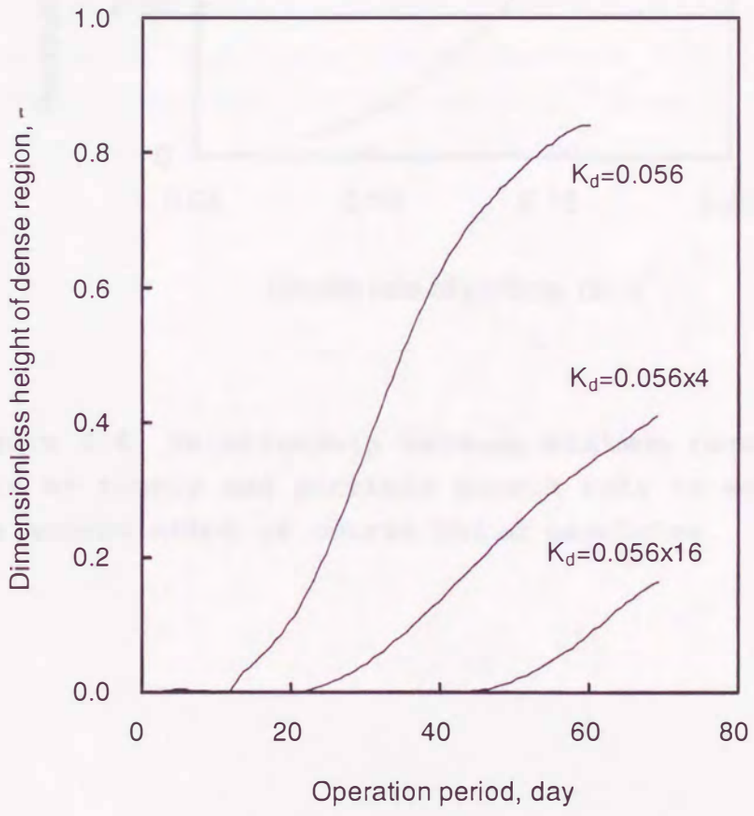

Figure 6-7. Effect of axial dispersion coefficient on the dimensionless heights of the dense region in the first reactor.

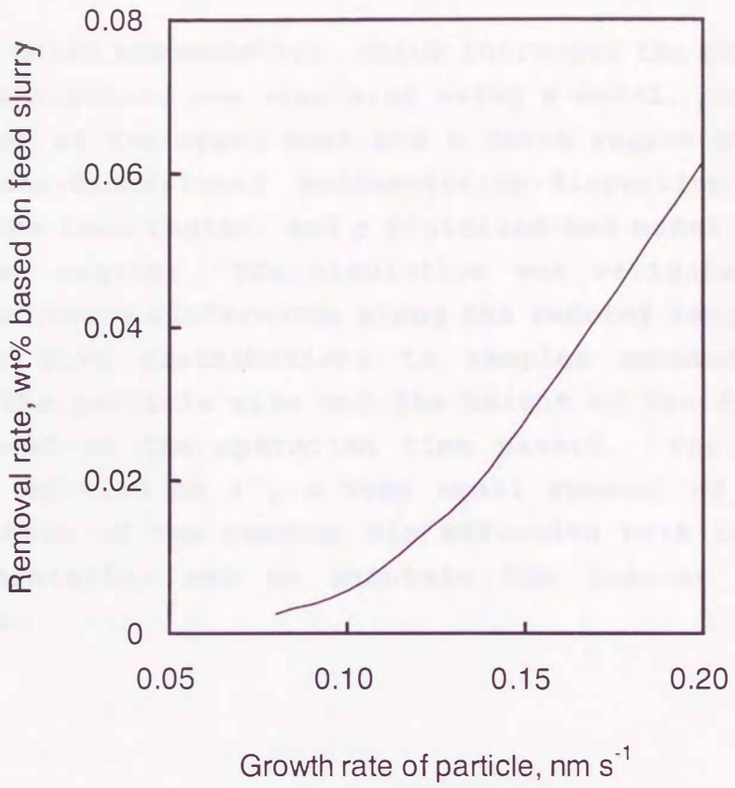

Figure 6-8. Relationship between minimum removal rate of slurry and particle growth rate to avoid the accumulation of coarse solid particles.

6.7 Conclusions

The solid accumulation, which increased the pressure drop in the first reactor, was simulated using a model, consisting of a lean region at the upper part and a dense region at the lower part. A one-dimensional sedimentation-dispersion model was applied to the lean region, and a fluidized-bed model was applied to the dense region. The simulation was validated from the changes in pressure differences along the reactor length, as well as particle size distributions in samples removed from the reactors. The particle size and the height of the dense region were increased as the operation time passed. For a particle growth rate of 0.10 nm s^{-1}, a very small removal of the slurry from the bottom of the reactor was effective both to avoid the solid sedimentation and to maintain the reactor volume for liquefaction.

Nomenclature

C = concentration of solid particles, kg m^{-3}

D_t = diameter of reactor, m

E_l, E_p = axial dispersion coefficients of liquid and solid particles, m^2 s^{-1}

F = slurry flow rate, m^3 s^{-1}

f_D = correction factor of Equation (20)

G_q = volumetric flow rate of quench gas, m^3(STP) s^{-1}

G_r = volumetric flow rate of recycle gas, excluding gas and oil vapor which are evolved by reactions, m^3(STP) s^{-1}

g = gravity constant, m s^{-2}

K_g = growth rate of solid particle, nm s^{-1}

K_p = correction factor of Equation (24)

L_f = mass flow rate of makeup slurry, kg s^{-1}

H = effective length of the reactor including top and bottom portions, m

H_d = height of dense region, m

Q = solid ratio in slurry phase, -

S = concentration of solid particles in slurry phase, kg m^{-3}

t = time, s

U = liner velocity of slurry, m s^{-1}

U_g, U_l, U_{sl} = superficial velocity of gas, liquid, and slurry, m s^{-1}

U_p = sedimentation velocity of a particle, m s^{-1}

U_t = terminal velocity of a particle, m s^{-1}

V = volume of reactor, m^3

W = the amount of coarse particles in the reactor, kg

x = axial position, m

y = coordinate of diameter of a particle, m

ΔP = pressure difference along the reactor length, kPa

ε_g, ε_{sl}, ε_s = gas, slurry, and solid holdup

μ_l = viscosity of liquid, kg m s^{-1}

ρ_g, ρ_{sl}, ρ_s = density of gas including oil vapor, that of slurry including fine particles, and that of coarse solid particles, kg m^{-3}

Subscripts

b = isolated bubble

D = dense region

F = feed

g, l, sl, s = gas, liquid, slurry and solid phase, respectively

L = lean region

n, n+1 = particle size at n and n+1 step, respectively

p = particle

T, R = position of outflow and removal

t = pseudo-steady state at time t

References

(1) Ueda, S.; Aramaki, T.; Kobayashi, M. Study on solid deposit appeared in hot high pressure separator in coal liquefaction 150t/d pilot plant. *1999 Intern. Conf. Coal Sci., Taiyuan, Shanxi*, **1999**.

(2) Aramaki, T.; Namiki, Y.; Onozaki, M.; Takagi, T.; Ueda, S.; Kobayashi, M.; Mochida, I. Solid deposit found in 150t/d pilot plant of coal liquefaction (III), minerals found in the reactors and their roles in the precipitation of minerals in the downstream unit. *J. Japan Inst. Energy* **2000**, in press.

(3) Aramaki, T.; Onozaki, M.; Takagi, T.; Kamada, M.; Ueda, S.; Kobayashi, M.; Mochida, I. Solid deposit found in 150 t/d Pilot Plant of coal liquefaction, Solid deposit in hot high pressure separator (I). *J. Japan Inst. Energy* **1999**, *78*, 929-942.

(4) Wakeley, L. D.; Davis, A.; Jenkins, R. G.; Mitchell, G. D.; Walker, P. L. Jr. The nature of solids accumulated during solvent refining of coal. *Fuel* **1979**, *58*, 379-385.

(5) Okuma, O.; Yanai, S.; Yasumuro, M.; Makino, E. Scales and sediments formed during liquefaction of Victorian brown coal with a 50 ton (dry coal)/day pilot plant. *J. Japan Inst. Energy* **1999**, *78*, 332-344.

(6) Mochizuki, M.; Imada, K.; Inokuchi, K.; Nogami, Y. Operational analysis and development of coal liquefaction 1 t/d process supporting unit. *J. Japan Inst. Energy* **1997**, *76*, 1074-1083.

(7) Morooka, S.; Kato, Y.; Ikejiri, S.; Nakajima, M.; Matsuyama, H. Preliminary Simulation of Ash Accumulation in Dissolver of Direct Coal Liquefaction. *J. Chem. Eng. Japan* **1986**, *19*, 137-139.

(8) Onozaki, M.; Namiki, Y.; Kobayashi, M.; Morooka, S. A simulation of the accumulation of solid particles in coal liquefaction reactors based on the NEDOL process. *Ind. Eng. Chem. Res.* **1999**, submitted.

(9) Kato, Y.; Morooka, S.; Kago, T.; Saruwatari, T.; Yang, S. Axial holdup distributions of gas and solid particles in three-phase fluidized bed for gas-liquid (slurry)-solid systems. *J. Chem. Eng. Japan* **1985**, *18*, 308-313.

(10) Sakai, N.; Onozaki, M.; Saegusa, H.; Ishibashi, H.; Hayashi, T.; Kobayashi, T.; Tachikawa, N.; Ishikawa, I.; Morooka, S. Characterization of fluid dynamics in coal liquefaction reactors

using Neutron Absorption Tracer Technique. *AIChE J.* **1999**, submitted.
(11) Hidaka, N.; Onitani, M.; Matsumoto, T.; Morooka, S. Axial mixing and segregation of multicomponent coarse particles fluidized by concurrent gas-liquid flow. *Chemical Engineering Science* **1992**, *47*, 3427-3434.
(12) Kato, Y.; Nishiwaki, A.; Fukuda, T.; Tanaka, S. The behavior of suspended solid particles and liquid in bubble columns. *J. Chem. Eng. Japan* **1972**, *5*, 112-118.
(13) Irvine, A. R.; Cochran, H. D.; Culberson, O. L.; Fisher, J. F.; Gambill, W. R.; Oswald, G. E.; Salmon, R. *Direct liquefaction technology assessment. Task 1. Technical readiness of the developing plant functions.* Oak Ridge National Laboratory, ORNL/TM-9181, 1985.
(14) Matsumoto, T.; Hidaka, N.; Takebayashi, Y.; Morooka, S. Axial mixing and segregation in gas-liquid-solid three-phase fluidized bed of solid particles of different sizes and densities. *Chemical Engineering Science* **1997**, *52*, 3961-3970.

7. A Process Simulation of the NEDOL Coal Liquefaction Process

7.1 Introduction

Large-scale coal liquefaction plants called a demonstration plant have been conceptually designed by process developers[1-3]. Regarding the SRC-II process, each unit model including a kinetic model in a reactor was developed and then the overall plant simulation was performed[4]. The recycle model for a heavy fraction was also developed[5]. Through these studies based on the performance of pilot and bench scale plant data, yield data for a large-scale plant were determined to do process design of process units including liquefaction reactors. However, differences in operation conditions exist, as a result of the philosophy of the processes.

The objectives of the present study[6] are to analyze the performance in the Kashima pilot plant using Tanitoharum coal, and to develop a design procedure for a large scale plant based on the NEDOL process. The reaction simulator used to estimate the yields in the liquefaction reactors was validated via the use of reaction kinetics data and vapor-liquid equilibria, which were obtained at the Kashima pilot plant.

7.2 Liquefaction Yields in the Kashima pilot plant

The reaction simulator, CARD[7], can be applied to predict the yields of the Kashima pilot plant. The following assumptions are made.

(i) The plant processes 150 tons of dry coal per day.

(ii) The reactor system consists of three backmix-type vessels connected in series. There are no temperature differences among the gas, liquid and solid particles in each reactor. The continuous stirred tank reactor (CSTR) model is adopted in the present calculation, since the simulator contains a number of parameters which should be decided.

(iii) The vapor and liquid phases are in equilibrium.

(iv) Liquefaction proceeds only in the slurry phase, in which the pyrite catalyst resides.

(v) The volume of the slurry phase in the reactor is calculated from the gas holdup given by Equation (5) in Section 2.4.

The liquefaction consists of 13 reaction steps from coal to gas, three fractions of oil (oil #1, C_4 to BP = 493 K; oil #2, BP = 493-623 K; oil #3, BP = 623-811 K), and a residue including ash and catalyst. The reaction scheme is shown in Figure 7-1. A portion of coal, denoted as C_A, is rapidly liquefied to asphaltenes, preasphaltenes, heavy oil (BP = higher than 811 K; referred to as PAAO), oil #3 and CO, CO_2, H_2O. The reaction rate for the path from a portion of coal, which is denoted as C_B, to PAAO (reaction rate constant, K_1) is considerably lower than that from C_A to PAAO (reaction rate constant, k_{CA}). C_i represents the non-reactive portion of the coal. The PAAO fraction is hydrogenated to H_2O, gas, oil #1, and oil #3, which is a precursor of oil #2. The hydrogenation from oil #2 to oil #1 is neglected, since most of oil #1 is produced directly from the PAAO. These reactions are irreversible except for the water-gas shift reaction.

The reaction rate coefficient of each reaction was determined from the yields of the process supporting unit (PSU, capacity = 1 ton of coal per day)[8], which was constructed and operated based on the NEDOL Process using Tanitoharum coal. The

physical properties of the coal liquids were obtained using the products of the Kashima pilot plant as described above. Vapor-liquid equilibria were calculated using the SRK equation[9] and were verified using data obtained from the high pressure separator of the PSU.

For case 2 of Table 2-2, the total oil yield calculates to be 49 wt%, which is less than the experimental value of 51 wt%. This difference may be due to errors in calculation in the mean residence time of the slurry in the reactor. However, the correction of vapor-liquid equilibria is rather complicated. For simplicity, therefore, the total calculated oil yield is adjusted to the experimental value using a correction factor with respect to the reactor length, defined as follows:

(effective reactor height)/(actual reactor height; 11.8 m).(1)

As shown in Figure 7-2 (a), the correction factor is 1.08 for case 2. It is noteworthy that the gas and residue yields, as well as the hydrogen consumption, are in agreement with the data when the reactor height is corrected as above.

For case 4 of Table 2-2, on the other hand, the correction factor is 0.92 as shown in Figure 7-2 (b). However, it was found that 18 % of the reactor volume of the first reactor was occupied with the accumulated solids in case 4. Thus the net volume fraction of the slurry phase for case 4 should be reduced by 6 % from the volume fraction calculated from $(1-\varepsilon_g)$. The correction factor is then 0.98, after the reactor volume is adjusted by the accumulation of solid particles.

The mean residence time of the slurry phase ascending through the three reactors at the Kashima pilot plant, as calculated from the simulator, is 4400 s for case 2 and 6000 s for case 4. The mean residence time of the slurry phase was also determined by the neutron absorption tracer technique, to be 5100 s for case 1 and 7200 s for case 4. The experimental data of the mean residence time are longer than the calculated values for both cases. However, the discrepancies, which may be attributed to errors in calculation of vapor-liquid equilibria, are sufficiently small to predict the gas and oil yields in the large-scale reactors.

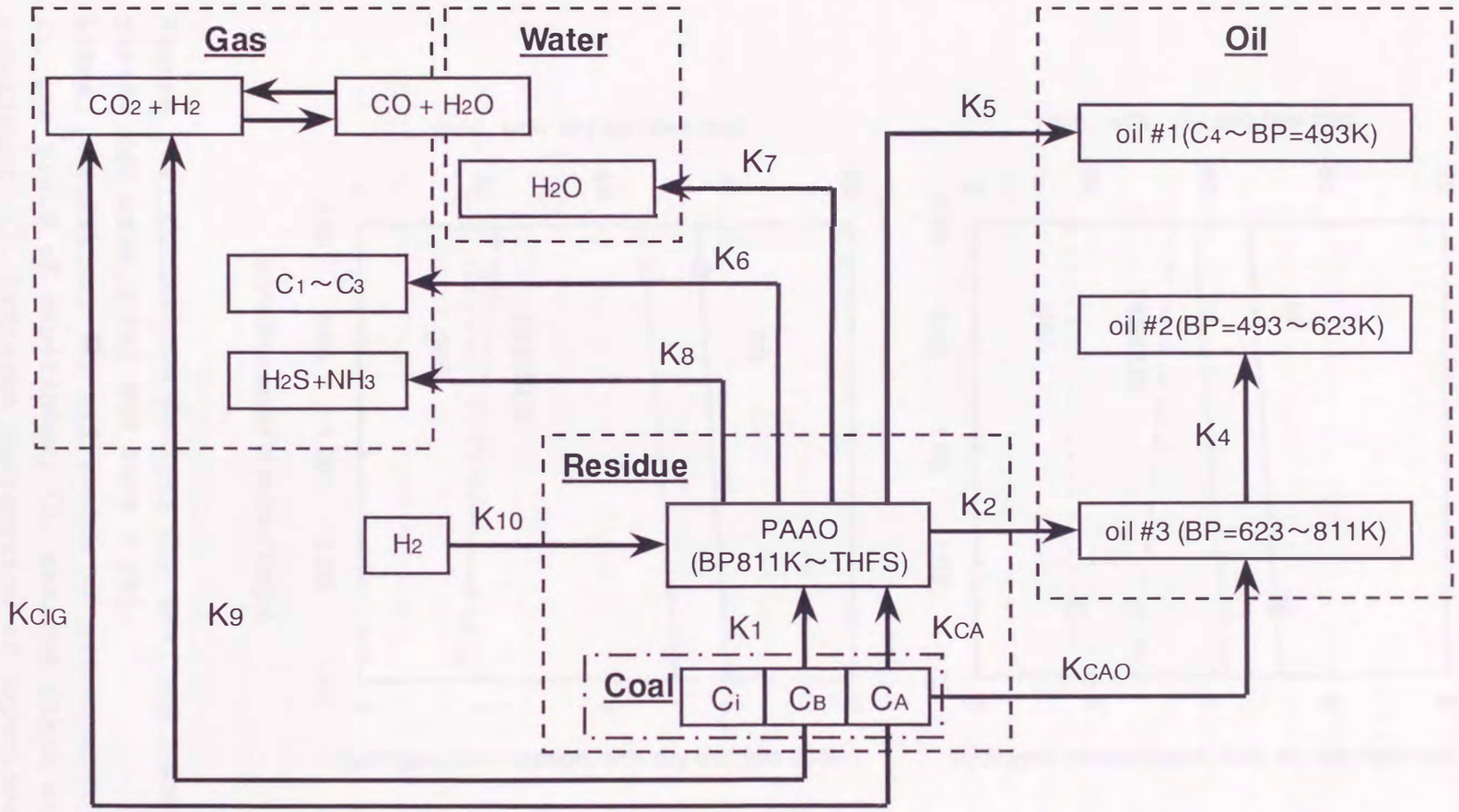

Figure 7-1. Assumed reaction paths in the simulator model.

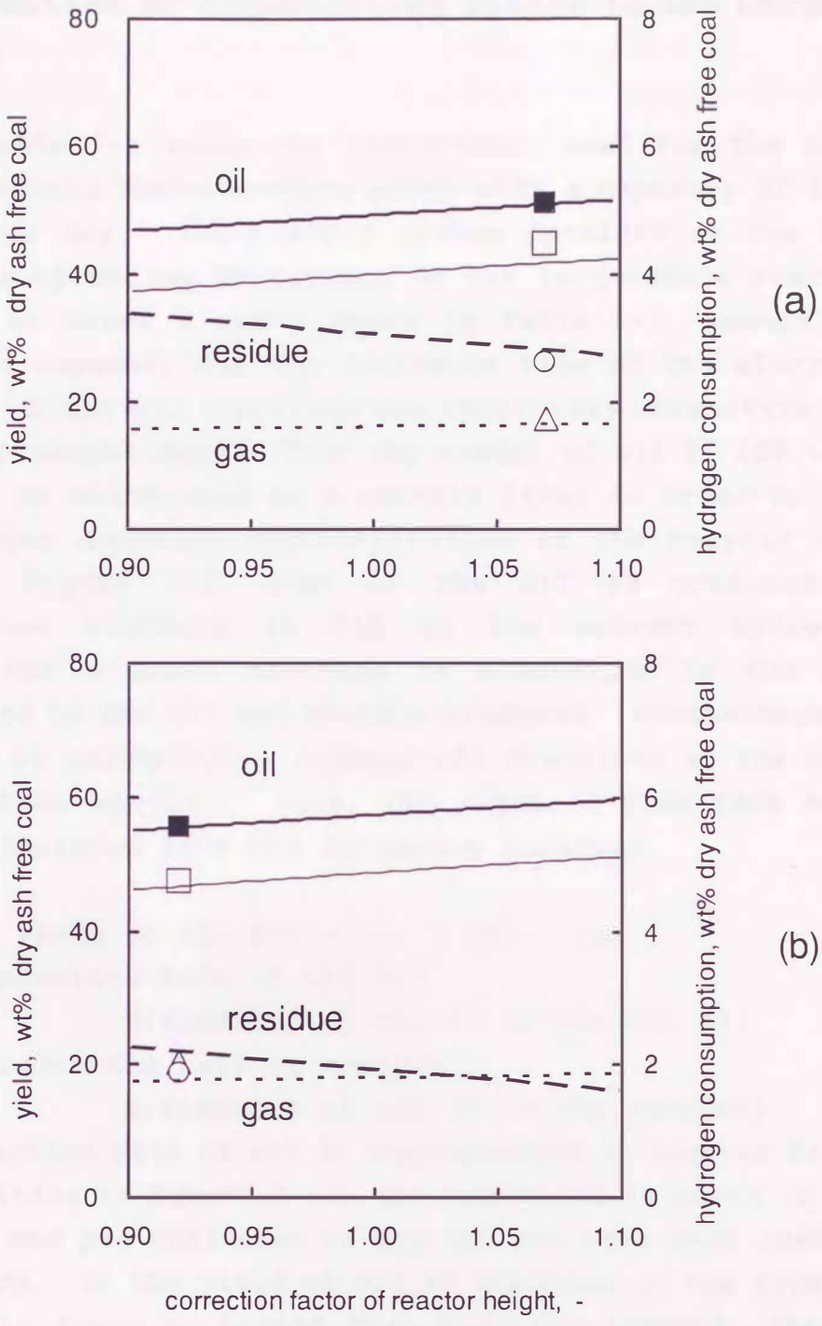

Figure 7-2. Correction factors for gas, oil, and residue yields for case 2 (a) and case 4 (b).
Lines, simulation; ■, oil yields of experiment; △, gas yield of experiment; ○, residue yield of experiment; □, hydrogen consumption of experiment.

7.3 Estimation of Liquefaction Yields in the Large-scale Reactors

Table 7-1 shows the conditions, used for the design of the large-scale demonstration plant with a capacity of 2500 tons of coal per day. The reactor system consists of two or three CSTRs. The operating conditions of the large-scale reactors are the same as cases 2 and 4 shown in Table 2-2, except for the production capacity and the residence time of the slurry in the reactors. Light oil fractions are relatively unreactive with the coal and preasphaltene. Thus the amount of oil #3 (BP = 623-811 K) should be maintained at a certain level in order to preserve the hydrogen donation characteristics of the recycle oil. As shown in Figure 7-3, most of the oil #3 produced in the liquefaction reactors is fed to the solvent hydrogenation section, but a small fraction is discharged to the outside, accompanied by the oil and residue produced. Furthermore, a part of oil #3 is converted to lighter oil fractions at the catalytic hydrogenation section. Thus, the required feed rate of oil #3 can be calculated from the following balance;

(required yield of oil #3) = (a) + (b) + (c) (2)

(a) = (production rate of oil #2)
x(fraction of oil #3 to the oil #2)

(b) = (production rate of residue)
x(fraction of oil #3 in the residue)

(c) = (reaction rate of oil #3 hydrogenated to lighter fractions)

All quantities in Equation (2) are expressed in units of mass per unit time and per unit mass of dry and ash free coal (daf) in the feed slurry. If the yield of oil #3 produced in the liquefaction reactors is lower or higher than this requirement, the recycle oil becomes lighter or heavier during the long-term operation of the liquefaction. Each term in the right-hand side of Equation (1) is estimated as follows:

(a) The fraction of oil #3 contained in the outflow as oil #2 is assumed to be 5 wt% from the engineering experience of the petroleum atmospheric fractionators.

(b) Although the content of oil fractions in the residue should be as low as possible to achieve a higher oil recovery yield, the softening point of the residue should be at least lower than 445 K. Figure 7-4 shows the relationship between the softening temperature (determined by a ring-and-ball method, ASME D36-95) and the hexane soluble content of the residue. In order to assure smooth handling, the softening point of the residue is assigned to be 435 K, which is 10 K lower than the limit. Thus the content of oil #3 in the residue is assumed to be 8 wt%.

(c) The severity of the hydrogenation section should be increased when a slurry is prepared with a higher coal concentration, as in case 4. Thus the oil #3 yield, which is decreased in the hydrogenation section, is increased for the high concentration slurry. Based on the data in the Kashima pilot plant, the decrease in the oil #3 yield in the hydrogenation section is assumed to be 3.2 wt% for case 2 (coal concentration = 40 wt%) and 7.2 wt% for case 4 (coal concentration = 48.5wt%).

Table 7-1. Design parameters for a large-scale demonstration plant

	case 2	case 4
Recycle gas		
Averge molecular weight	5.5	5.5
Fraction of hydrogen, vol%	86	86
Makeup slurry		
Coal feed rate, kg/h, dry coal basis	104200	104200
Recycle oil in slurry,	156300	104200
Catalyst (pyrite powder) in slurry, wt%, dry coal basis	3	3
Reaction		
Operating pressure, MPa	16.6-16.8	16.6-16.8
Operating temperature, top of the two reactors, K	728	733
G_r/L_f *, m^3(STP)/kg-slurry	0.70	0.90

* (volumetric flow rate of total recycle gas fed to the two reactors)/(mass flow rate of makeup coal slurry)

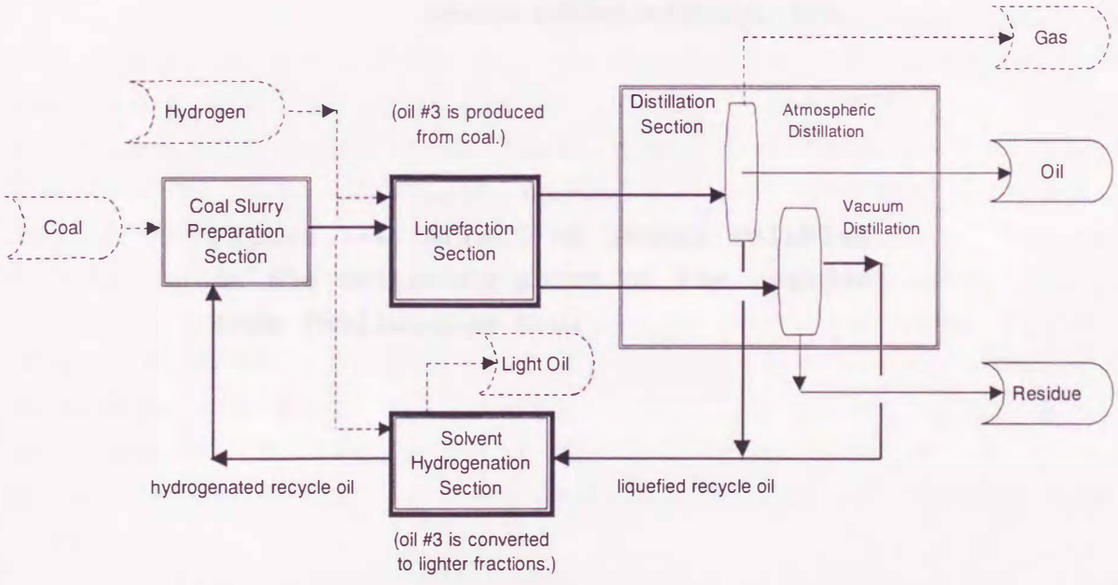

Figure 7-3. Flow chart of the NEDOL process. Solid lines, stream containing oil #3; broken lines, streams with no oil #3.

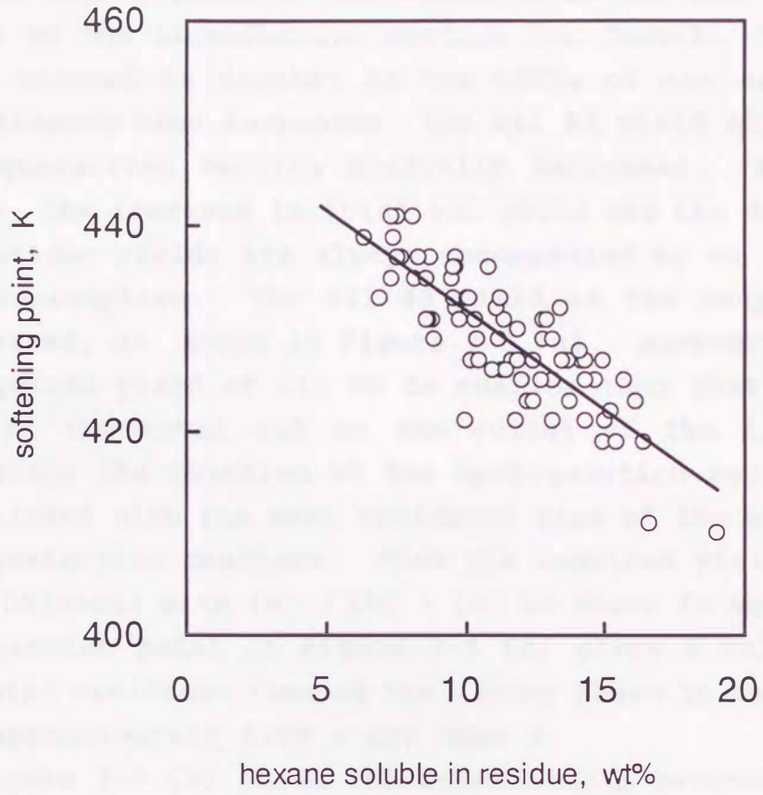

Figure 7-4. Effect of hexane solubles on the softening point of the residue from Tanitoharum coal.

Figure 7-5 (a) shows the effect of the mean residence time of the slurry phase in the reactors on the oil #3 yield at the outlet of the liquefaction section for case 2. The reactor system is assumed to consist of two CSTRs of the same volume. As the residence time increases, the oil #3 yield at the outlet of the liquefaction section gradually decreases. As shown in Figure 7-6, the increase in total oil yield and the decreases in gas and residue yields are always accompanied by an increase in hydrogen consumption. The oil #3 yield in the recycle oil is also decreased, as shown in Figure 7-5 (a). However, the slope of the required yield of oil #3 is smaller than that of the oil #3 yield in the total oil at the outlet of the liquefaction section, since the reaction at the hydrogenation section is not directly linked with the mean residence time of the slurry phase in the liquefaction reactors. Thus the required yield of oil #3 should be balanced with (a) + (b) + (c) as shown in Equation (2). The intersection point in Figure 7-5 (a) gives a value for the optimum total residence time of the slurry phase in the reactors, which is approximately 5100 s for case 2.

Figure 7-5 (b) shows the relationship between the total oil yield at the outlet of the reactor system and the total residence time of the slurry phase. The total oil yield increases with increasing total residence time of the slurry phase. The total oil yield, which is calculated for the reactor system with three CSTRs, is also shown in the figure. In this calculation, the total residence time is equally divided into the three reactors. The total oil yield in the three CSTR system is higher than that in the two CSTR system, but the difference is approximately 1 wt%. This suggests that the effect of the number of reactors, providing the total residence time of the slurry phase is the same, is not appreciable for two versus three CSTRs.

Figure 7-7 (a) shows the relationship between the oil #3 yield and the total residence time of the slurry phase for case 2, shown in Table 7-1. The oil #3 yields are optimized at a mean residence time of 7500 s. The total oil yield is 59 wt% on a dry and ash free coal basis, and 5.0 wt% of the hydrogen on a dry and

ash free coal basis is consumed in the liquefaction reactors. Figure 7-7 (b) shows the effect of the number of reactors on the total oil yield for case 4. The result is similar to case 2. The product yields which are estimated for cases 2 and 4 are shown in Table 7-2.

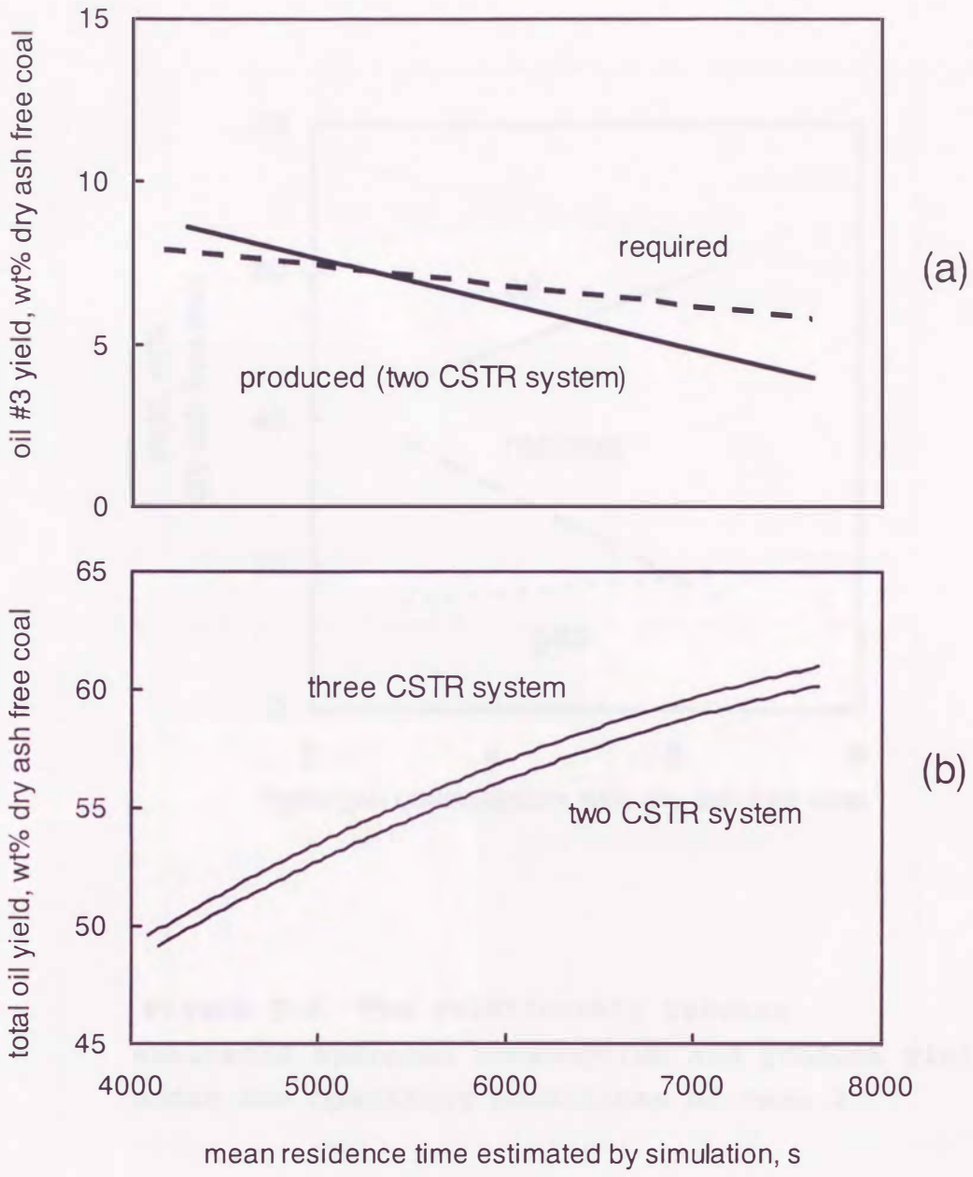

Figure 7-5. Effect of slurry residence time on oil #3 yield (a) and total oil yield (b) for case 2.

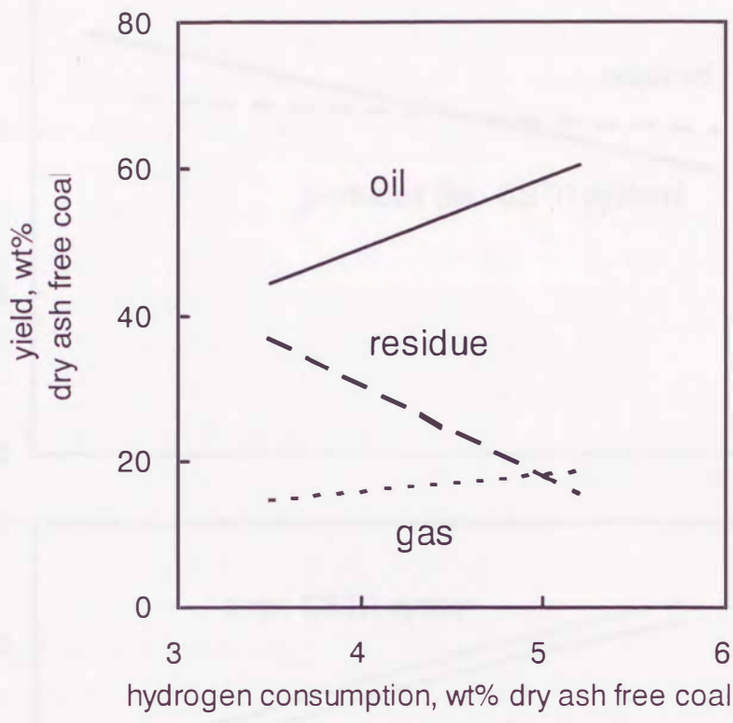

Figure 7-6. The relationship between estimated hydrogen consumption and product yields under the operating conditions of case 2.

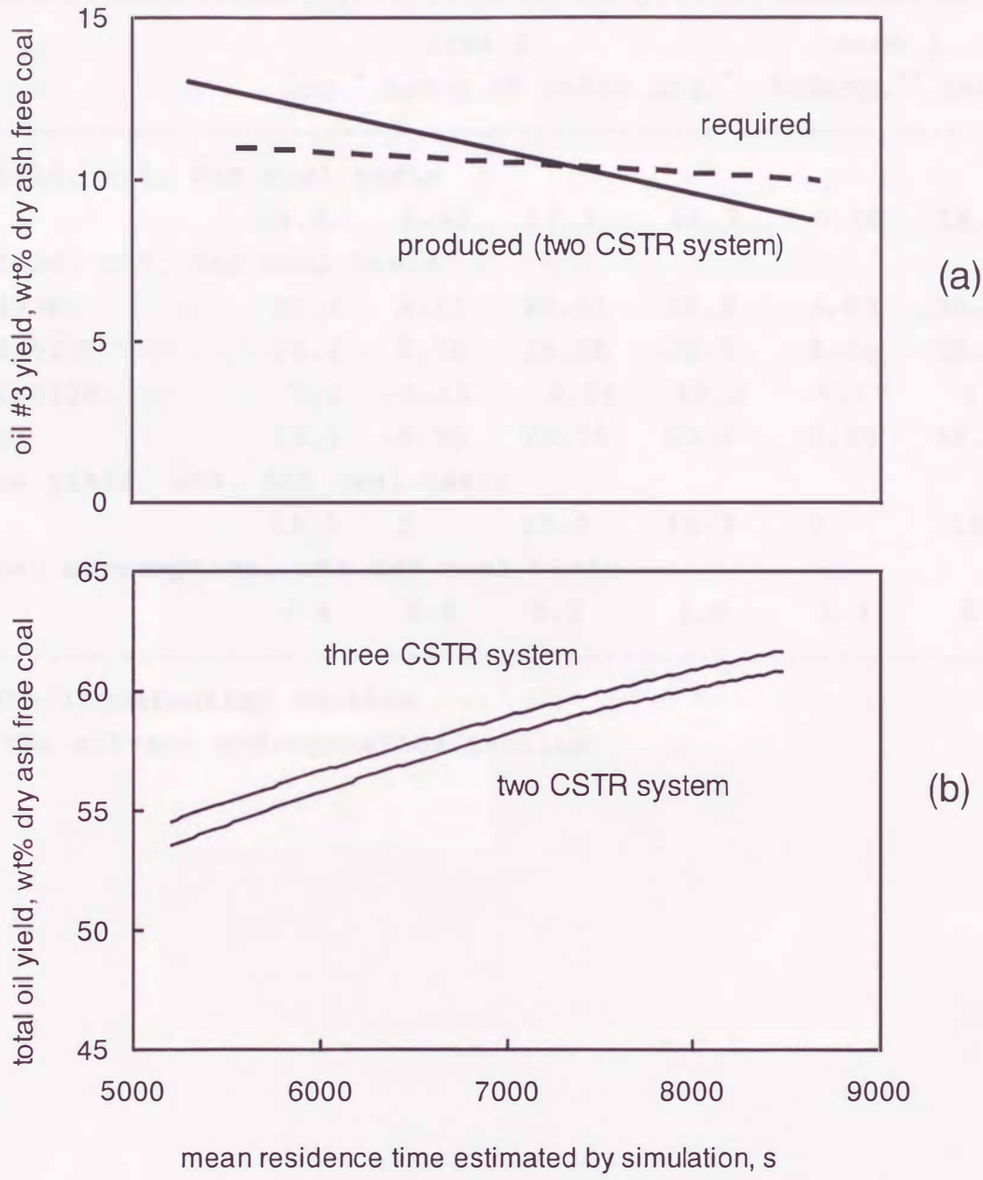

Figure 7-7. Effect of slurry residence time on oil #3 yield (a) and total oil yield (b) for case 4.

Table 7-2. Estimated yields of liquefaction and solvent hydrogenation sections

	case 2			case 4		
	liq.*	hydrg.**	total	liq.*	hydrog.**	total
Gas yield, wt%, daf coal basis						
	16.8	0.45	17.3	18.7	0.78	19.5
oil yield, wt%, daf coal basis						
C4-493K	27.8	2.11	29.91	26.2	3.83	30.03
493K-623K	18.1	0.70	18.80	22.7	2.54	25.24
623K-811K	7.2	-3.16	4.04	10.3	-7.17	3.13
Total	53.1	-0.35	52.75	59.2	-0.80	58.40
Residue yield, wt%, daf coal basis						
	25.5	0	25.5	16.7	0	16.7
hydrogen consumption, wt% daf coal basis						
	4.4	0.8	5.2	5.0	1.3	6.3

* in the liquefaction section

** in the solvent hydrogenation section

7.4 Conclusions

The product yields of the Kashima pilot plant and the large-scale plant were predicted using a simulator developed for the NEDOL process. The compositions and physical properties of the recycle oils obtained in the PSU and the Kashima pilot plant were applied to these calculations. The yield of oil #3 in the recycle oil was a key determinant in maintaining the hydrogen donor ability of the recycle oil. The total residence time of the slurry phase in the reactors was determined from this requirement. The total oil yield was not greatly changed for the reactor systems with two versus three CSTRs.

References

(1) Pittsburg & Midway Coal Mining Xo. *SRC-II demonstration project, Phase zero Task No.3 Conceptual commercial plant summary.* FE-3055-T2 (Vol. 1), 1979.
(2) Catalytic Inc. *6000 TPD SRC-I demonstration plant. Design baseline. Volume I-VI.* DOE-OR-3054-T-26-VOL-1,2,3,4,5,6, 1982.
(3) Ashland Synthetic Fuels, Inc.; Airco Energy Co., Inc. *The Breckinbridge Project, Initial Effort, Report 1, Executive summary.* DOE/OR/20717-1, DE83 000177.
(4) Singh, C.P.P.; Carr, N.L. Process simulation of an SRC-II. *Ind. Eng. Chem. Process Des. Dev.* **1983**, *22*, 104-118.
(5) Singh, C.P.P.; Shah, Y.T.; Carr, N.L. Liquefaction of coal by SRC-II process, Part II: Simulation of an SRC-II recycle system. *The Canadian Journal of Chemical Engineering* **1982**, *60*, 261-271.
(6) Onozaki, M.; Namiki, Y.; Ishibashi, H.; Kobayashi, M.; Itoh, H., Hiraide, M.; Morooka, S. A process simulation of the NEDOL coal liquefaction process. *Fuel Processing Technology*, **2000**, in press.
(7) Hiraide, M.; Itoh, H.; Kidoguchi, A.; Kaneda, E.; Kobayashi, M.; Namiki, Y.; Imada, Y.; Inokuchi, K. Coal Liquefaction reactor simulator. *Proc. Int. Symp. Fundamentals for Innovative Coal Utilization, Sapporo*, **1999**, 103-106.
(8) Mochizuki, M; Imada, K.; Ikeda, K.; Inokuchi, K.; Nogami, Y.; Takeda, T.; Sakawaki, K. Study of fluid dynamics in coal liquefaction reactor. *Proc. of 4th Japan/German Symp. On Bubble Columns, Kyoto,* 1997, 393-400.
(9) Soave, G. Equilibrium constants from a modified Red-Kwong equation of state. *Chemical Engineering Science* **1972**, *27,* 1197-1203.

8. Scale-up of Coal Liquefaction Reactors

8.1 Introduction

Large-scale liquefaction reactors based on several processes have been conceptually designed[1-3]. The proposed EDS process[1] involves a plug flow-type reactor of 2.9 m in diameter and 47.5 m in height, having a capacity of 6300 tons of Illinois #6 coal per day. The proposed SRC-II process[2] involves a backmixed-type reactor of 3.35 m in diameter and 20.4 m in height with a capacity of 1500 tons of coal per day. However, differences in reactor designs and operation conditions exist, as a result of the philosophy of the processes.

The objectives of the present study[4,5] are to develop a design procedure for large-scale liquefaction reactors based on the NEDOL process, which would have a capacity of 2500 tons of coal per day. The dimensions of the reactors are discussed based on the yield data and the required residence time in the reactors determined in Chapter 7.

8.2 Large-scale Reactors

The liquefaction reactors are bubble columns for gas, liquid and solid systems. The gas phase consists largely of hydrogen, which is introduced into the reactor as bubbles, acts as a reactant in the liquefaction process, and causes the mixing of the slurry phase. The gas phase also contains light hydrocarbons, which are produced by liquefaction. Coal is disintegrated into small particles in the preheating section, and the fine particles of coal, ash and catalyst are homogeneously suspended in the liquid. This slurry phase resides in the reactors for approximately one hour. After a lengthy operation, however, coarse particles are formed and accumulate in the reactors[6]. It is defined in this article that the coarse particles are not included in the slurry phase, which thus consists of only the liquid and fine particles.

Two extreme mixing conditions in a bubble column reactor are possible; backmix flow and plug flow. Large-scale reactors are assigned to the backmix flow. Since coal liquefaction is highly exothermic, the heat of reaction should be compensated for by quenching gas or liquid, which is introduced into the reactors. In a backmix flow, the temperature of the feed slurry rapidly reaches a prescribed value after the slurry is introduced into the reactor. Thus, the temperature at the outlet of the preheater can be maintained at a value, which is lower than the temperature in the reactor and is determined from a balance with the heat production in the first reactor. A reduction in the preheater outlet temperature is useful to avoid coking, which is possible at temperatures over 680 K.

On the other hand, a plug flow reactor minimizes the reactor volume. Direct coal liquefaction involves multi-step conversions of coal to preasphaltenes and asphaltenes, and then to gas, oil and residue[7]. A plug flow reactor will bring higher yields of the intermediate components. However, a considerable temperature distribution may be formed in each reactor. As a result, a quench is often required to control the heat, which is generated by the liquefaction reaction. A multi-staged reactor

system is a compromise between both flow types, but the optimum number of reactors which can be connected in series is strongly dependent on the design concept of the plant.

If liquefaction yields are controlled by reaction rates in a backmix-flow or plug-flow reactor, which is mainatined at a prescribed temperature, the mean residence time of the slurry phase in the reactor is only the design parameter. Thus the scale-up of the reactor is performed via each of the following principles.

(i) The aspect ratio of the reactor is maintained, and the slurry velocity is increased.

(ii) The reactor diameter is increased, and the slurry velocity is maintained.

When the degree of mixing in the reactor is intermediate, however, gas and slurry velocities, as well as reactor dimensions, influence the temperature and the reactant concentrations along the axial positions in the reactor.

The gas holdup in the reactors at the Kashima pilot plant is estimated to be 0.45-0.60 as mentioned in Section 2.4. A gas holdup of 0.5-0.6 is likely to be the maximum for a homogeneous bubble flow[8]. Thus, the superficial gas velocity of the large-scale reactors cannot be increased beyond the value of the Kashima pilot plant, if the homogeneous bubble flow regime is to be maintained in the large-scale reactors, as in the Kashima pilot plant.

The above discussion suggests that the reactor diameter can be increased in accord with increasing feed rate. Since the ratio of the recycle gas to the feed slurry, G_r/L_f, is determined by the required hydrogen supply and the vaporization of product oil, the sectional area of the reactor will be in proportion to the amount of coal which is processed. When the total height of the reactor and the superficial gas velocity are maintained at the approximate values of the Kashima pilot plant, the mass transfer rate of gaseous hydrogen to the liquid phase will not be very different for the large-scale reactors. If the large-scale reactors are constructed using the 3Cr-1Mo-1/4V-Ti-B alloy (ASME code; SA336-F3V), which was developed by NEDO, and

using a stainless steel 347 overlay, the maximum inner diameter of the reactor will be limited to approximately 5 m. This is dictated by currently used manufacturing techniques. The maximum capacity per each train of reactors (5 m in diameter) is then 25 fold larger than the Kashima pilot plant and is capable of processing 4000 tons of coal per day. In the following part of this study, the hydrodynamic and physical properties in the large-scale reactors with a diameter of 4 m (capacity = 2500 tons of coal per day) will be discussed.

8.3 Hydrodynamics in the Large-scale Reactors

8.3.1 Gas Holdup

The correlation of the gas holdup with a gas superficial velocity was proposed based on the Kashima pilot plant data in Section 2.4.

Only limited data are available for a large-scale bubble column with more than 1-m diameter. Koide et al.[9] reported that the effect of superficial gas velocity on gas holdup in a 5.5-m diameter bubble column (approximately 4 m in height) was nearly the same as in small-size bubble columns operated under ambient conditions. Wilkinson et al.[10] also discussed the design parameters of bubble columns at elevated pressures based on the data of 0.15-0.61 m diameter column and concluded that the gas holdup was virtually independent of column dimension and sparger layout, provided the following criteria were fulfilled,

(i) diameter > 0.15 m,

(ii) ratio of height to diameter (aspect ratio) > 5, and

(iii) sparger hole size > 1-2 mm.

All these conditions will be satisfied in the large scale liquefaction reactors.

8.3.2 Flow Regime

The Kashima pilot plant was operated without hydrodynamic instability at superficial gas velocities of 0.05-0.085 m s^{-1}. The axial dispersion coefficients of the liquid (slurry) phase were determined as mentioned in Section 2.5 by a neutron absorption tracer technique. The small values observed suggest that a homogeneous bubble flow regime prevailed at superficial gas velocities less than 0.075 m s^{-1}. In the reactors of a brown coal liquefaction pilot plant in Victoria, Australia[11], the gas holdup was approximately 0.68 at superficial gas velocities of 0.10-0.16 m s^{-1}. The axial dispersion coefficient of the liquid phase increased from 0.13 to 0.25 m^2 s^{-1} with increasing gas velocity. These data suggest that the flow regime in the brown coal liquefaction reactors is assigned to the homogeneous bubble flow regime with some disturbances. Letzel et al.[12] investigated

the effect of pressure on flow in a bubble column for the nitrogen-water system at elevated pressures ranging 0.1 to 0.9 MPa. The homogeneous bubble flow was changed to the heterogeneous bubbly flow regime at a superficial gas velocity of 0.08-0.10 m s^{-1} at 0.9 MPa. From the above data, it can be assumed that the homogeneous bubble flow regime is maintained in the large-scale reactors, provided the superficial gas velocity is less than 0.085 m s^{-1}. However, a certain amount of turbulence can be expected, depending on the physical properties of the gas and slurry, the aspect ratio of the reactors, and the temperature profile in the reactors.

8.3.3 Axial Dispersion Coefficient

As mentioned in Chapter 3, f_D in equation (10) was determined by the temperature profiles to be 0.088. In Chapter 6, f_D was determined by the measured axial dispersion coefficients to be 0.056. 0.088 is more accurate for the thermal study, because it was determined by containing many unknown factors on heat transfer.

No data is available for the dispersion coefficient of a bubble column with more than 1 m in diameter at elevated pressures. Even under ambient conditions, only limited data exist. In a larger size, such as 2 to 4 m in diameter, f_D defined by the following equation is supposed to be constant with water-air or nitrogen systems under ambient conditions as can be seen in Figure 8-1.

$$f_D = \frac{E_l}{U_g^{0.3}} \qquad (1)$$

f_D = 0.678 in Figure 8-1 means the coefficient of a 1-m diameter column determined by Deckwer et al.[15]. Thus, it is highly likely that the measured value by the Kashima pilot plant can be applied to a larger-scale reactor without serious difference.

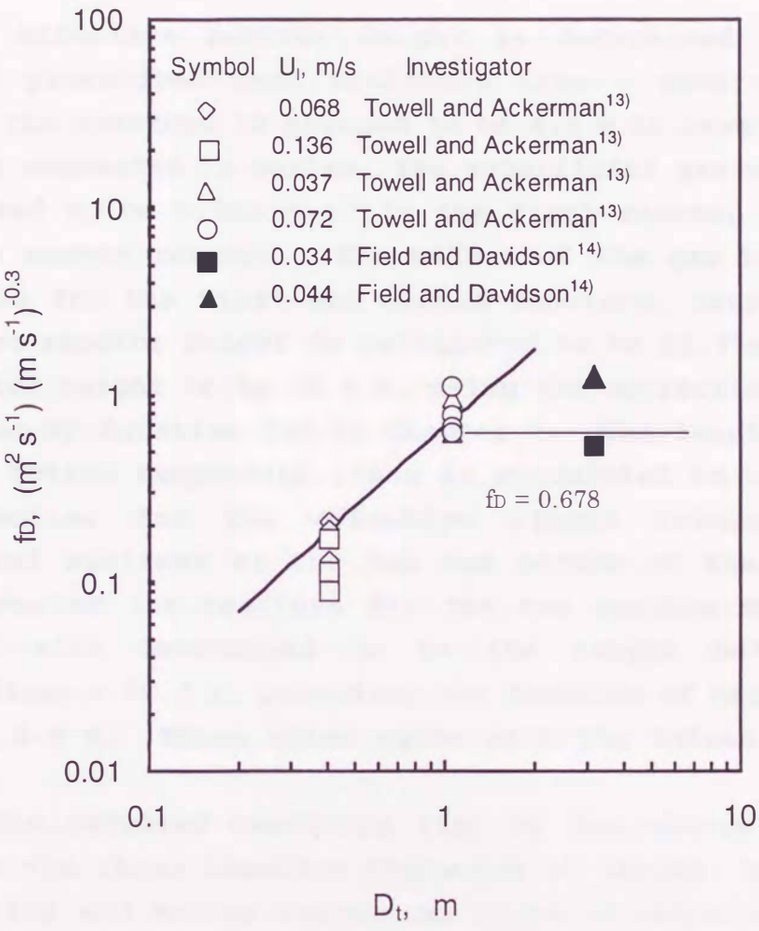

Figure 8-1. Effect of diameter on axial liquid dispersion coefficient.

8.4 Dimensions of the Large-scale Reactors

The effective reactor height is determined so as to satisfy the prescribed mean residence time. When the inner diameter of the reactors is assumed to be 4.0 m in case 2 for the two reactors connected in series, the superficial gas velocities are calculated to be 0.058 m s^{-1} in the first reactor and 0.077 m s^{-1} in the second reactor. The values of the gas holdup are 0.52 and 0.59 for the first and second reactors, respectively. The effective reactor height is calculated to be 23.7 m, and the actual reactor height to be 21.9 m, using the correction factor, 1.08, defined by Equation (1) in Chapter 7. The length between the top and bottom tangential lines is calculated to be 20.7 m, after correction for the effective liquid volume in the semi-spherical sections at the top and bottom of the reactor. The dimensions of the reactors for the two reactor system for case 4 are also determined to be the length between the tangential lines = 20.7 m, providing the diameter of the reactors is fixed as 4.0 m. These sizes agree with the values for case 2 by chance.

If the required residence time of the slurry phase is divided into the three reactors connected in series, the length between the top and bottom tangential lines is calculated to be 14.4 m. As shown in Figure 7-5, however, the total oil yield is not greatly different for the systems with two versus three reactors. Thus, the number of reactors should be determined from the viewpoints of aspect ratio, maximum size for manufacturing and transportation, stable introduction of feed and quench, etc. The aspect ratio of each reactor for the three reactor systems is as low as 3, which may cause unstable flows of gas and slurry phases in the reactors. Moreover, the two reactor system can reduce the cost for equipment and construction in comparison with the three reactor system. If the dimensions of the reactors which are connected in series are not limited by local conditions of the construction site, the two reactor system is more advantageous than the three reactor system.

8.5 Thermal Behavior in the Large-scale Reactors

In order to establish the steady-state operation of liquefaction plants, design items with respect to thermal stability, such as feed temperature, locations of quench gas injection, amounts of quench gas and liquid, and thermal dispersion in the reactors, need to be more fully examined.

The axial dispersion model stated in Section 3-2 was applied to a large-scale reactor system consisting of two reactors in series. The design conditions for the thermal simulation are shown as case 2 in Table 7-1. The heat of reaction, the heat loss per the shell surface, and the correlation of the gas holdup used in Chapter 3 were adopted. The flow rates of quench gas are dependent on the feed temperature to the first reactor to maintain the top temperature to the designated value, satisfying the heat balance of the reactor system. The lower feed temperature gives the lower bottom temperature of the first reactor, which may suppress the exothermic reaction. The higher feed temperature causes increase of the flow rates of the quench gas and results in the lower thermal efficiency of the system. In the Kashima pilot plant, the lowest temperature at the bottom part of the first reactor through the steady operation in case 2 was 696 K, maintaining the top temperature to 728 K. The ratio of the axial distance with the lower temperature than the designated value and the total length has to be less than 1/3 to apply the model, because only the temperatures in the first reactor were over three K less than 728 K in the Kashima pilot plant. Considering these conditions, one example of the feed temperature, locations of quench gas injection, amounts of quench gas, and temperature profiles is shown in Table 8-1 and Figure 8-1.

Table 8-1. Design conditions and simulation results for a large-scale reactor system with two reactors in series

	Case 2
Operating pressure, MPa	16.6-16.8
Operating temperature,	
feed of the first reactor, K	678
bottom of the first reactor, K	693
top of the first reactor, K	728
bottom of the second reactor, K	727
top of the second reactor, K	728
G_r/L_f^*, m^3(STP) kg^{-1}-slurry	
at the feed line	0.50
G_q/L_f^* of the first reactor, m^3(STP) kg^{-1}-slurry	
at 0.59 of dimensionless height from the bottom	0.075
at 0.82 of dimensionless height from the bottom	0.05
G_q/L_f^{**} of the second reactor, m^3(STP) kg^{-1}-slurry	
at 0.25 of dimensionless height from the bottom	0.025
at 0.50 of dimensionless height from the bottom	0.025
at 0.75 of dimensionless height from the bottom	0.025
Calculated axial dispersion coefficient	
at the first reactor, m^2 s^{-1}	0.041
at the second reactor, m^2 s^{-1}	0.043

* (volumetric flow rate of recycle fed to the feed slurry)/(mass flow rate of makeup coal slurry)

** (volumetric flow rate of quench gas at the position)/(mass flow rate of makeup coal slurry)

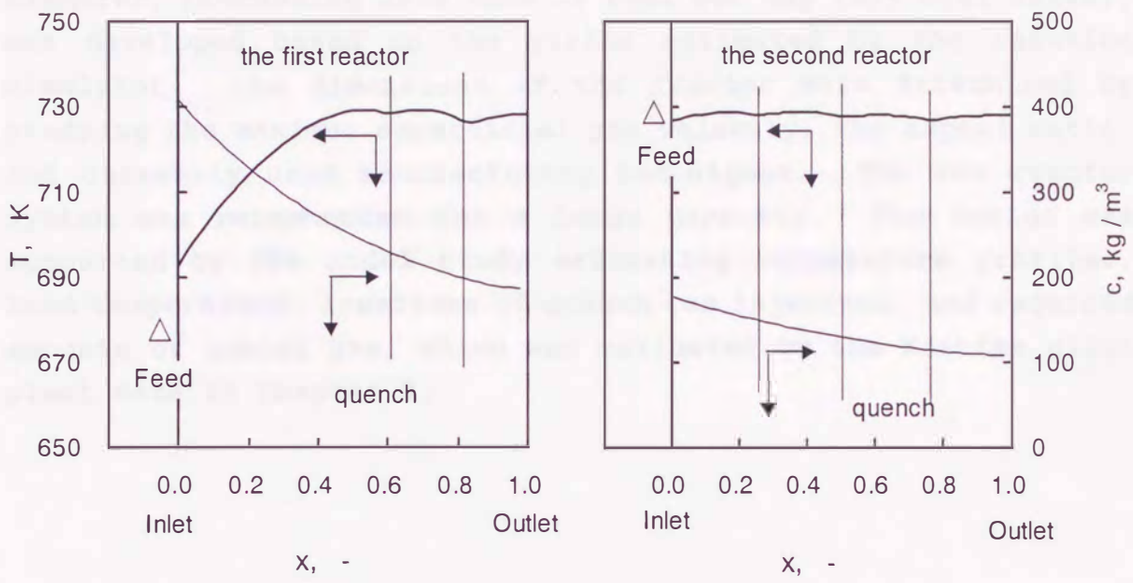

Figure 8-2. Calculated temperature profiles in large-scale reactors (case 2).

8.6 Conclusions

The procedure for designing the reactors of 4 m in diameter, processing 2500 tons of coal per day (dry coal basis), was developed based on the yields estimated by the reaction simulator. The dimensions of the reactor were determined by studying the maximum superficial gas velocity, the aspect ratio, and currently used manufacturing techniques. The two reactor system was recommended for a large capacity. The design was supported by the model study estimating temperature profiles, feed temperature, locations of quench gas injection, and required amounts of quench gas, which was validated by the Kashima pilot plant data in Chapter 3.

Nomenclature

c = concentration of reactant, kg m^{-3}
D_t = diameter of column, m
E_l = axial dispersion coefficient of liquid, m^2 s^{-1}
f_D = correction factor defined by Equation (1)
G_q = volumetric flow rate of quench gas, m^3(STP) s^{-1}
G_r = volumetric flow rate of recycle gas, excluding gas and oil vapor which are evolved by reactions, m^3(STP) s^{-1}
L_f = mass flow rate of makeup slurry, kg s^{-1}
U_g, U_l = superficial velocity of gas and liquid, m s^{-1}
x = axial position from the bottom, -

References

(1) Irvine, A. R.; Cochran, H. D.; Culberson, O. L.; Fisher, J. F.; Gambill, W. R.; Oswald, G. E.; Salmon, R. *Direct liquefaction technology assessment. Task 1. Technical readiness of the developing plant functions.* Oak Ridge National Laboratory, ORNL/TM-9181, 1985.

(2) Irwin, C.F.; Sincali, A.J.; Wong, E.W. *Hydrodynamics of coal-liquefaction dissolver configurations,* Oak Ridge National Laboratory, ORNL/MIT-326, 1981.

(3) Exxon Research and Engineering Company, *EDS consolidation programme, reactor optimization design study, Phase V,* FE-2893-152, 1985.

(4) Onozaki, M.; Namiki, Y.; Ishibashi, H.; Kobayashi, M.; Itoh, H., Hiraide, M.; Morooka, S. A process simulation of the NEDOL coal liquefaction process. *Fuel Processing Technology*, **2000**, in press.

(5) Onozaki, M.; Namiki, Y.; Takagi, T.; Kobayashi, M.; Itoh, H.; Hiraide, M. Scale-up of Coal Liquefaction Reactor of NEDOL Process. *Proc. of 16th International Annual Pittsburgh Coal Conference, Pittsburgh* **1999**, No. 28-2.

(6) M. Onozaki, Y. Namiki, T. Aramaki, T. Takagi, M. Kobayashi, S. Morooka, *Ind. Eng. Chem. Res.*, submitted for publication.

(7) Shah, Y.T. *Reaction Engineering in Direct Coal Liquefaction*; Addison-Wesley Publishing Co.: Massachusetts, 1981.

(8) Tarmy, B.L.; Chang, M.; Coulaloglou, C. A.; Ponzi, P. R. The three phase hydrodynamics of the EDS coal liquefaction reactors: their development and use in reactor scaleup. *Inst. Chem. Eng., Sym. Ser.* **1984**, No.87, 303-317.

(9) Koide, K.; Morooka, S.; Ueyama, K.; Matsuura, A.; Yamashita, F.; Iwamoto, S.; Kato, Y.; Inoue, H.; Shigeta, M.; Suzuki, S.; Akehata, T. Behavior of bubbles in large scale bubble column. *J. Chem. Eng. Japan* **1979**, *12*, 98-104.

(10) Wilkinson, P.M.; Spek, A.P.; van Dierendonck, L.L. Design parameters estimation for scale-up of high-pressure bubble columns. *AIChE J.* **1992**, *38*, 544-554.

(11) Tanaka, Y.; Tamura, M.; Kageyama, H.; Clark, K. Fluid dynamics studies in the brown coal liquefaction reactor. *2nd Japan/Australia Joint Technical Meeting on Coal, Tokyo*, **1992**, 198-204.

(12) Letzel, H.M.; Schouten, J.C.; van der Bleek, C.M.; Krishna, R. Influence of elevated pressure on the stability of bubbly

flows. *Chemical Engineering Science* **1997**, *52*, 3733-3739.
(13) Towell, G.D.; Ackermann,G.H. *Proc. of 5th Europe/2nd Int. Symp. Chem. React. Eng., Amsterdam,* **1972**, B3-1.
(14) Field, R. W.; Davidson, J. F. Axial dispersion in bubble column. *Trans IchemE* **1980**, *58*, 228-236.
(15) Deckwer, W.D.; Burckhart, R.; Zoll, G. Mixing and mass transfer in tall bubble columns. *Chemical Engineering Science* **1974**, *29*, 2177-2188.

9. Conclusions

A coal liquefaction pilot plant having a capacity of 150 tons of coal per day was successfully operated from 1996 to 1998 at Kashima, Japan. The hydrodynamics and thermal behavior of the three liquefaction reactors connected in series, each of which was 1 m in diameter and 11.8 m in length, were investigated. By means of the model studies validated by the data obtained on the Kashima pilot plant, the design procedure of the liquefaction reactors, which would be 4 m in diameter and process 2500 tons of coal per day, was developed.

In Chapter 2, the correlation of the gas holdup, which highly affects the reactor volume, was proposed based on the pilot plant data. No effect of the diameter on the gas holdup was found at superficial gas velocities lower than 0.07 m s^{-1}. The axial dispersion coefficients under the liquefaction conditions determined by the neutron absorption tracer technique were one order of magnitude smaller than those for air-water systems at ambient pressure and temperature and 1/3-1/6 of those obtained for the cold oil.

In Chapter 3, an axial dispersion model considering the heat of reaction was applied to the reactor and validated by the steady-state temperature profiles in the reactor. The estimated dispersion coefficients were close to those determined by the neutron absorption tracer technique.

In Chapter 4, the results of the computational fluid dynamics suggest that the axial dispersion coefficient is not greatly increased even if the diameter of the reactor is increased to four times that of the Kashima pilot plant. The predicted flow patterns show that the temperature difference between the top and the bottom of the reactor, as well as the introduction of the cold quench gas, was effective at decreasing the axial dispersion coefficient of the liquid.

In Chapter 5, the coarse solid particles accumulated in the first reactor were investigated. Two types of solid particles were produced, i.e., particles without cores, and particles with cores. The cores were largely composed of SiO_2. The particles grew in size by additional deposition of mainly Ca onto the cores, and the growth rate of the particles in the first

reactor was determined to be 10 nm s^{-1}.

In chapter 6, the solid accumulation, which increased the pressure drop in the first reactor, was simulated using a model, consisting of a lean region at the upper part and a dense region at the lower part. The removal of a very small amount of the slurry from the bottom of the reactor was effective both at avoiding solid sedimentation and at maintaining the reactor volume for liquefaction.

In Chapter 7, the product yields of the Kashima pilot plant and the large-scale plant were predicted using the reaction simulator developed for the NEDOL process. The yield of a heavy fraction in the recycle oil was a key determinant in maintaining the hydrogen donor ability of the recycled oil. The total residence time of the slurry phase in the reactors was determined from this requirement.

In chapter 8, the procedure for designing the 4 m diameter reactors to process 2500 tons of coal per day, was developed based on the yields estimated by the reaction simulator. The design was supported by the model study estimating the thermal behaviors.

The hydrodynamics and performance data of the pilot plants constructed and operated in the U.S.A. had been fragmentarily reported. In this study, these data were combined with the data obtained in the Kashima pilot plant and a scale-up procedure of the liquefaction reactors has been developed by the model studies including reaction and thermal analyses and computational fluid dynamics. If the yield and physical property data are obtained for even a new kind of coal by a small-scale test unit, this study will greatly contribute to designing a large-scale plant for such a potential project.

Acknowledgment

I would like to express my sincere appreciation to Professor Shigeharu Morooka for his helpful guidance and invaluable suggestion for this study at Department of Materials Physics and Chemistry, Graduate School of Engineering, Kyushu University.

I would like to express my gratitude to Professor Katsuhiko Wakabayashi, Department of Materials Process Engineering, and to Professor Hisayoshi Matsuyama, Department of Chemical System and Engineering, Graduate School of Engineering, Kyushu University, for their reviewing this thesis and giving critical comments.

In addition, acknowledgment of the support of Mr. Masatoshi Kobayashi, my boss, and many colleagues of Nippon Coal Oil Co., Ltd. in offering many constructive suggestions as well as the operation data for analysis is hereby made. The financial support of the New Energy and Industrial Technology Development Organization (NEDO) in line with the New Sunshine Project is gratefully appreciated. Without meeting Dr. C.Y. Wen of blessed memory in Morgantown, West Virginia, U.S.A., twenty years ago, coal liquefaction might not have been my research theme. Last, but not least, such a research could never have been successfully completed without love and sacrifice from my family and particularly my wife.

Masaki Onozaki

March, 2000

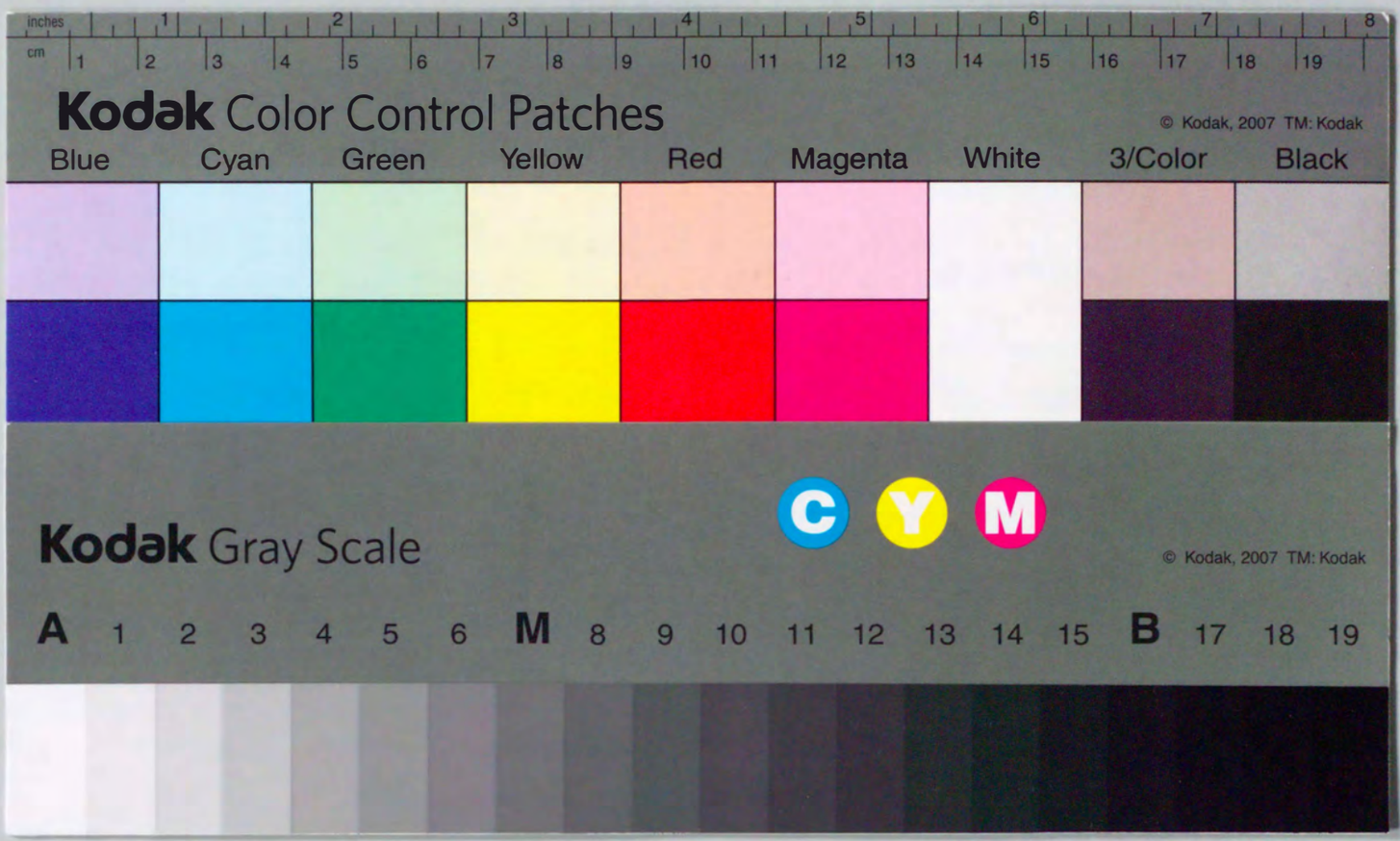
inches
cm
Kodak Color Control Patches
© Kodak, 2007 TM: Kodak
Blue
Cyan
Green
Yellow
Red
Magenta
White
3/Color
Black
Kodak Gray Scale
C
Y
M
© Kodak, 2007 TM: Kodak
A 1 2 3 4 5 6 M 8 9 10 11 12 13 14 15 B 17 18 19